

Nitrification and nitrous oxide production in the offshore waters of the Eastern Tropical South Pacific

Alyson E Santoro¹, Carolyn Buchwald², Angela N Knapp³, William M. Berelson⁴, Douglas G. Capone⁴, and Karen L Casciotti⁵

¹University of California Santa Barbara

²Dalhousie University

³Florida State University

⁴University of Southern California

⁵Stanford University, Department of Environmental Earth System Science

November 23, 2022

Abstract

Marine oxygen deficient zones (ODZs) are dynamic areas of microbial nitrogen cycling. Nitrification, the microbial oxidation of ammonia to nitrate, plays multiple roles in the biogeochemistry of these regions, including production of the greenhouse gas nitrous oxide (N₂O). We present here the results of two oceanographic cruises investigating nitrification, nitrifying microorganisms, and N₂O production and distribution from the offshore waters of the Eastern Tropical South Pacific (ETSP). On each cruise, high-resolution measurements of ammonium ([NH₄⁺]), nitrite ([NO₂⁻]), and N₂O were combined with ¹⁵N tracer-based determination of ammonia oxidation, nitrite oxidation, nitrate reduction and N₂O production rates. Depth-integrated inventories of NH₄⁺ and NO₂⁻ were positively correlated with one another, and with depth-integrated primary production. Depth-integrated ammonia oxidation rates were correlated with sinking particulate organic nitrogen flux but not with primary production; ammonia oxidation rates were undetectable in trap-collected sinking particulate material. Nitrite oxidation rates exceeded ammonia oxidation rates at most mesopelagic depths. We found positive correlations between archaeal genes and ammonia oxidation rates and between -like 16S rRNA genes and nitrite oxidation rates. N₂O concentrations in the upper oxycline reached values of greater than 140 nM, even at the western extent of the cruise track, supporting air-sea fluxes of up to 1.71 μmol m⁻² d⁻¹. Our results suggest that a source of N₂O other than ammonia oxidation may fuel high rates of nitrite oxidation in the offshore ETSP and that air-sea fluxes of N₂O from this region may be higher than previously estimated.

1 **Nitrification and nitrous oxide production in the offshore waters of**
2 **the Eastern Tropical South Pacific**

3
4
5 Alyson E. Santoro^{1*}, Carolyn Buchwald², Angela N. Knapp³, William M. Berelson⁴, Douglas
6 G. Capone⁵, Karen L. Casciotti⁶
7
8
9

10
11 ¹Department of Ecology, Evolution, and Marine Biology, University of California, Santa
12 Barbara, California, USA; ²Department of Oceanography, Dalhousie University, Halifax, Nova
13 Scotia, Canada; ³Earth, Ocean, and Atmospheric Science Department, Florida State
14 University, Tallahassee, Florida, USA; ⁴Department of Earth Sciences, University of Southern
15 California, Los Angeles, California, USA; ⁵Department of Biological Sciences, University of
16 Southern California, Los Angeles, California, USA; ⁶Department of Earth System Science,
17 Stanford University, Stanford, CA, USA
18

19
20 *Corresponding author: Alyson E. Santoro (asantoro@ucsb.edu)
21
22

23 **Key points:**
24

- 25 • Depth-integrated ammonia oxidation rates are correlated with sinking particulate
26 nitrogen flux, indicating substrate supply as a primary control of water column
27 nitrification.
28
- 29 • Nitrous oxide (N₂O) is produced from ammonium (NH₄⁺) in the water column, with an
30 instantaneous N₂O yield from nitrification (N₂O-N/NO₃⁻) lower than previous
31 estimates.
32
- 33 • Higher than anticipated N₂O concentrations were measured in offshore waters, which
34 may arise from local production, leading to large air-sea fluxes of N₂O.
35
36
37

38 Running head: *Nitrification in the offshore ETSP*

39 **Abstract**

40

41 Marine oxygen deficient zones (ODZs) are dynamic areas of microbial nitrogen cycling.
42 Nitrification, the microbial oxidation of ammonia to nitrate, plays multiple roles in the
43 biogeochemistry of these regions, including production of the greenhouse gas nitrous oxide
44 (N_2O). We present here the results of two oceanographic cruises investigating nitrification,
45 nitrifying microorganisms, and N_2O production and distribution from the offshore waters of
46 the Eastern Tropical South Pacific (ETSP). On each cruise, high-resolution measurements of
47 ammonium ($[\text{NH}_4^+]$), nitrite ($[\text{NO}_2^-]$), and N_2O were combined with ^{15}N tracer-based
48 determination of ammonia oxidation, nitrite oxidation, nitrate reduction and N_2O production
49 rates. Depth-integrated inventories of NH_4^+ and NO_2^- were positively correlated with one
50 another, and with depth-integrated primary production. Depth-integrated ammonia oxidation
51 rates were correlated with sinking particulate organic nitrogen flux but not with primary
52 production; ammonia oxidation rates were undetectable in trap-collected sinking particulate
53 material. Nitrite oxidation rates exceeded ammonia oxidation rates at most mesopelagic
54 depths. We found positive correlations between archaeal *amoA* genes and ammonia
55 oxidation rates and between *Nitrospina*-like 16S rRNA genes and nitrite oxidation rates. N_2O
56 concentrations in the upper oxycline reached values of >140 nM, even at the western extent
57 of the cruise track, supporting air-sea fluxes of up to $1.71 \mu\text{mol m}^{-2} \text{d}^{-1}$. Our results suggest
58 that a source of NO_2^- other than ammonia oxidation may fuel high rates of nitrite oxidation in
59 the offshore ETSP and that air-sea fluxes of N_2O from this region may be higher than
60 previously estimated.

61

62

63 **Keywords**

64 Ammonia oxidation, nitrite oxidation, nitrate reduction, nitrous oxide, oxygen deficient zones

1. Introduction

Marine oxygen deficient zones (ODZs) are dynamic areas of microbial nitrogen cycling. In the four major oceanic ODZs, oxygen (O_2) concentrations in the water column are low enough to allow the microbial nitrogen removal processes of denitrification and anaerobic ammonium oxidation (anammox) (Devol, 2008). Together these two processes set the fixed nitrogen inventory of the ocean by returning biologically fixed nitrogen back to N_2 gas. Nitrification, the microbial oxidation of ammonia (NH_3) to nitrite (NO_2^-) and ultimately nitrate (NO_3^-), plays an important role in linking nitrogen inputs and losses in ODZs because it produces the substrates necessary for denitrification and anammox (Lam *et al.*, 2007; Ward *et al.*, 2009).

Aside from its role as a link between sources and sinks in the nitrogen cycle, nitrification plays other important roles in marine biogeochemistry. First, nitrification may influence estimates of nitrate-driven 'new' production by providing a recycled source of NO_3^- within the euphotic zone (Dugdale and Goering, 1967). Second, ammonia oxidation, the first step of nitrification, evolves the long-lived greenhouse gas nitrous oxide (N_2O). N_2O production has been linked to the metabolism of both ammonia-oxidizing bacteria (AOB) (Goreau *et al.*, 1980) and ammonia-oxidizing archaea (AOA) (Löscher *et al.*, 2012; Santoro *et al.*, 2011). N_2O is correlated with apparent oxygen utilization (AOU), a measure of organic matter remineralization, and thus nitrogen remineralization, throughout the world's oceans, though with varying slopes (Nevison *et al.*, 2003). N_2O cycling is hypothesized to be dynamic at the fringes of ODZs, where N_2O may be both produced by ammonia oxidation and produced and consumed by denitrification (Babbín *et al.*, 2015; Cohen and Gordon, 1979; Ji *et al.*, 2015). The amount of N_2O cycling through each of these pathways, however, is poorly quantified as are the exact enzymatically and non-enzymatically catalyzed reactions leading to N_2O production during ammonia oxidation (Kozłowski *et al.*, 2016; Liu *et al.*, 2017). The fate of N_2O within ODZ waters has important implications for quantifying how much N_2O originating in the ODZ is eventually released to the atmosphere, where it contributes to both greenhouse warming and ozone depletion (Bianchi *et al.*, 2012; Martínez-Rey *et al.*, 2015; Yang *et al.*, in press).

The Eastern Tropical South Pacific (ETSP) is the second largest marine ODZ by area. While pioneering (Codispoti and Christensen, 1985; Lipschultz *et al.*, 1990; Ward *et al.*, 1989) and more recent (*e.g.*, (Bourbonnais *et al.*, 2015; Casciotti *et al.*, 2013; Kalvelage *et al.*, 2013; Lam *et al.*, 2009; Peng *et al.*, 2016)) field campaigns have brought attention to the dynamic nitrogen biogeochemistry in the ODZ core (from the Peruvian shelf out to approximately 85° W), less attention has been paid to offshore waters of the eastern Pacific, where low O_2 , relatively high $[NO_2^-]$, high N_2O waters impinge on the extremely oligotrophic waters of the south Pacific gyre. In these offshore waters, O_2 concentrations in most of the water column are higher than typically believed to permit water column denitrification, thought to initiate at $2.5 - 4.5 \mu\text{mol L}^{-1}$ (Bianchi *et al.*, 2012; Devol, 2008). These O_2 concentrations are low enough, however, to potentially influence the rate and efficiency of aerobic nitrogen cycling processes, such as nitrification (Bristow *et al.*, 2016), as well as support anaerobic nitrogen cycling processes within microenvironments on sinking particulate matter (Bianchi *et al.*, 2018). Low but non-zero O_2 concentrations may also influence the coupling of the two steps of nitrification (ammonia oxidation and nitrite oxidation), supporting a dynamic oxidation, reduction, re-oxidation loop with implications for the overall N and C stoichiometry of ODZs (Buchwald *et al.*, 2015; Granger and Wankel, 2016; Sigman *et al.*, 2005).

115 Recent studies have suggested that uncertainties in our ability to model and predict N₂O
116 emissions from the ocean result from a poor understanding of the quantitative relationship
117 between nitrification and N₂O production as a function of O₂ (Zamora *et al.*, 2012). This is
118 further complicated by uncertainties in the mechanisms by which N₂O is produced during
119 ammonia oxidation. It has been suggested that, because N₂O in AOA cultures may not form
120 directly from an enzymatic reaction, its production should not be influenced by ambient
121 oxygen concentration (Stieglmeier *et al.*, 2014). This is in direct contrast to empirical
122 observations, however, which clearly show dependence of N₂O yield (the amount of N₂O-N
123 produced for every mole of NO₂⁻ produced) on O₂ (Qin *et al.*, 2017). Indeed, recent
124 experiments have shown that N₂O production in the ocean, where AOA are the dominant and
125 often only ammonia oxidizers (Santoro *et al.*, 2010; Wuchter *et al.*, 2006), is tied to ammonia
126 oxidation and increases at low O₂ (Ji *et al.*, 2015; Ji *et al.*, 2018; Trimmer *et al.*, 2016).
127

128 We present here the results of two oceanographic cruises investigating nitrification and
129 nitrifying microorganisms in the offshore waters of the Eastern Tropical South Pacific (ETSP),
130 extending from the continental shelf out to 100°W. On each cruise, we determined rates of
131 ammonia oxidation, nitrite oxidation, and euphotic zone nitrate reduction using ¹⁵N tracers
132 and quantified the abundance of nitrifying organisms (AOB, AOA, and nitrite-oxidizing
133 bacteria, NOB) in the context of NO₂⁻, NH₄⁺, and N₂O distributions. We further quantified N₂O
134 production from NH₄⁺ and determined N₂O yield across environmental O₂ concentrations.
135 Finally, we coupled contemporaneous estimates of air-sea gas exchange to N₂O
136 concentration measurements to estimate the atmospheric flux of N₂O to the atmosphere.
137

138

139 **2. Methods**

140

141 **2.1 Cruise track and hydrography**

142

143 Sampling was conducted on two cruises to the ETSP in Feb-Mar 2010 ('Year 1') aboard the
144 R/V *Atlantis* (cruise AT15-61) and Mar-Apr 2011 ('Year 2') aboard the R/V *Melville* (cruise
145 MV1104). Both cruises were part of a larger project to quantify the impact of biological
146 nitrogen fixation and carbon export in this region of the ocean (Berelson *et al.*, 2015; Haskell
147 *et al.*, 2015; Knapp *et al.*, 2016). The cruise track in both years was a rectangular box,
148 occupying six major stations numbered counterclockwise (Fig. 1). The southern transect
149 extended along 20°S from 80°W to 100°W (Stations (Stns.) 1-5) and the northern transect
150 was along 10°S, from approximately 82.5°W to 100°W (Stns. 7-11). In both years,
151 hydrographic data were collected with using an SBE-9 profiling conductivity, temperature,
152 depth (CTD) sensor package (SeaBird Electronics) additionally equipped with a fluorometer
153 (Seapoint or WetLabs), transmissometer, a Clark-type electrode oxygen sensor (SBE 43,
154 SeaBird), and photosynthetically active radiation sensor (Biospherical/Licor). CTD sensor
155 data were processed using SeaSoft v7.2 (SeaBird) including application of the hysteresis
156 and tau corrections for deep water oxygen measurements (Edwards *et al.*, 2010).
157

158 Discrete water samples were collected using Niskin bottle-type rosette sampler equipped
159 with either (24) 10 L bottles or (12) 20 L Niskin bottles.
160

161 **2.2 Dissolved nutrient analyses**

162

163 Ammonium concentration ([NH₄⁺]) was determined on-ship in unfiltered 50 mL seawater
164 samples using o-phthaldialdehyde derivatization (Holmes *et al.*, 1999) and measurement on
165 an Aquafluor 8000 handheld fluorometer (Turner Designs), with modifications as suggested

166 in (Taylor *et al.*, 2007). Nitrite concentration ($[\text{NO}_2^-]$) was determined on-ship in unfiltered 50
167 mL sample volumes using standard colorimetric methods (Strickland and Parsons, 1968).
168 NH_4^+ standards (30 – 300 nM) were freshly prepared for each analysis in duplicate using
169 deep water (> 500 m) from the same station, which consistently had a lower blank than
170 ultrapure water. Samples for $[\text{NO}_2^- + \text{NO}_3^-]$ were stored frozen and determined in the
171 laboratory using vanadium reduction followed by chemiluminescence detection (Braman and
172 Hendrix, 1989), and $[\text{NO}_3^-]$ was calculated by difference. Detection limits for $[\text{NH}_4^+]$, $[\text{NO}_2^-]$,
173 and $[\text{NO}_3^-]$ were 10 nM, and 100 nM for both $[\text{NO}_2^-]$ and $[\text{NO}_3^-]$ analyses.
174

175 **2.3 Tracer-based rate measurements**

176 *2.3.1 Net primary production*

177 Net primary production (NPP) was determined in deckboard bottle incubations in both years.
178 In Year 1, for each depth, four 2 L polycarbonate bottles were filled directly from Niskin
179 bottles from a pre-dawn CTD rosette cast and amended with stable isotope-labeled sodium
180 bicarbonate ($\text{NaH}^{13}\text{CO}_3$) to a final concentration of 25 μM . A single bottle was filtered
181 immediately after isotope addition to establish an initial (T_0) atom% ^{13}C of the particulate
182 carbon for each depth. The remaining triplicate bottles were placed in surface seawater filled
183 circulating incubators and shaded by different mesh size combinations of aluminet screening
184 to simulate ambient light intensity. Incubations were carried out for ~24 h. All samples were
185 filtered onto precombusted (5 h at 400°C) 25 mm GF/F filters (Whatman), dried, and stored
186 until analysis on an IsoPrime continuous flow isotope ratio mass spectrometer at the
187 University of Southern California. In Year 2, NPP was determined with radiotracers (^{14}C)
188 using established protocols from the Bermuda Atlantic Time-Series and were previously
189 reported in (Knapp *et al.*, 2016).
190
191

192 *2.3.2 Ammonia and nitrite oxidation rates*

193 Ammonia and nitrite oxidation rates were determined using ^{15}N tracer additions (>98 atm%
194 $^{15}\text{NH}_4\text{Cl}$ or $\text{Na}^{15}\text{NO}_2^-$, Cambridge Isotope Laboratories). As described below, incubation
195 methods varied slightly between the first and second cruises.
196
197

198 In Year 1, rates were determined at four depths at all six stations, targeting the middle of the
199 euphotic zone, the primary nitrite maximum, the base of the euphotic zone, and the upper
200 oxycline. Incubations were conducted in 160 mL glass serum vials capped with 20 mm
201 diameter Teflon-backed gray butyl septa (Microliter Analytical, 20-0040AS) and sealed with
202 aluminum crimps. Bottles were filled from the Niskin sampling bottles using silicone tubing,
203 allowing approximately three volumes of sample water to overflow the bottle prior to
204 collection. Six serum bottles were filled and sealed from each incubation depth, spiked with
205 ^{15}N tracer (100-200 nM $^{15}\text{NH}_4\text{Cl}$ or $\text{Na}^{15}\text{NO}_2^-$) using a plastic syringe, and incubated in flowing
206 seawater incubators screened to mimic the *in situ* light environment (euphotic zone samples)
207 or temperature controlled chambers (sub-euphotic zone). Duplicate bottles were sacrificed at
208 timepoints of 0, 12, and 24 h from each incubation depth, 0.2 μm syringe-filtered into a 60 mL
209 HDPE bottle, and frozen at -20°C.
210

211 In Year 2, rates were determined at six depths at five stations between the middle of the
212 euphotic zone and 500 m depth. Due to undetectable rates encountered in the Year 1 cruise
213 at Stn 5 (see Results), no rates were determined at Stn 5 in Year 2. Incubations were
214 conducted in 500 mL Tedlar bags (Restek) equipped with a septum injection port and three-
215 way stopcocks for tracer addition and sampling, respectively. Bags were acid washed and
216

217 purged with N₂ between incubations. Duplicate incubation bags per treatment were filled from
218 the Niskin bottles using silicone tubing, and ¹⁵N tracer (200 nM ¹⁵NH₄Cl or Na¹⁵NO₂) was
219 added via the septum injection port. As in the previous year, bags were incubated at as close
220 to *in situ* light and temperature as possible. At timepoints of 0, 12, 24, and 36 h, 50 mL
221 samples were drawn from each bag through the three-way sampling port using a 60 mL
222 syringe while applying constant pressure to the incubation bag. At each timepoint, incubation
223 water was 0.2 μm syringe filtered into a 60 mL HDPE bottle tripled rinsed with sample, and
224 frozen at -20°C. At the conclusion of the experiment, the volume remaining in the bag was
225 drained into a graduated cylinder to calculate the initial seawater volume in the bag at the
226 beginning of the experiment.

227

228 Frozen samples were transported to the laboratory, thawed, and prepared for $\delta^{15}\text{N}_{\text{NO}_2+\text{NO}_3}$
229 analysis using the 'denitrifier method' (Sigman *et al.*, 2001) and analyzed on a custom purge
230 and trap system interfaced to a Thermo Delta Plus XP isotope ratio mass spectrometer
231 (IRMS) (McIlvin and Casciotti, 2011). For nitrite oxidation rate samples, the added ¹⁵NO₂⁻
232 tracer was removed using sulfamic acid addition and subsequent neutralization with NaOH
233 (Granger *et al.*, 2006) prior to sample preparation and analysis. For 2010 samples, where
234 only three timepoints were taken, rates were calculated using the linear fitting method of
235 Dugdale and Goering (Dugdale and Goering, 1967). For 2011, where four timepoints were
236 taken, rates were calculated using a least squares fitting approach that accounts for changes
237 in $\delta^{15}\text{N}_{\text{NO}_2+\text{NO}_3}$ from co-occurring nitrate uptake (Santoro *et al.*, 2010).

238

239 2.3.3 Nitrate reduction rates

240

241 Nitrate reduction rates to nitrite were determined in Year 2 using ¹⁵NO₃⁻ tracer additions (>98
242 atm% Na¹⁵NO₃, Cambridge Isotope Laboratories). Because our focus was on the potential
243 for NO₂⁻ production from assimilatory nitrate reduction by photoautotrophs and subsequent
244 leakage from cells (Lomas and Lipschultz, 2006), ¹⁵NO₃⁻ incubations were only conducted in
245 the euphotic zone (three depths) at the five stations where ammonia and nitrite oxidation
246 rates were made. Tedlar incubation bags were prepared and filled as above, and 200 or 400
247 nM (final concentration) of Na¹⁵NO₃ was added to each bag using a plastic syringe.
248 Timepoints were sampled and preserved as for the nitrification rate incubations above. In the
249 laboratory, samples were prepared for $\delta^{15}\text{N}_{\text{NO}_2}$ determination using the 'azide method'
250 (McIlvin and Altabet, 2005). Special sample handling and preparation were required to
251 analyze $\delta^{15}\text{N}_{\text{NO}_2}$ at the low concentrations encountered on the cruise, and to reduce the
252 possibility of ¹⁵NO₃⁻ contamination of the laboratory. Briefly, thawed samples with sufficient
253 NO₂⁻ (*i.e.* in samples where [NO₂⁻] was > 0.5 μM) were aliquoted into 20 mL glass vials at the
254 volume necessary to achieve 5 nmol NO₂⁻ analyte. Sargasso Sea surface water was then
255 added to a final volume of 10 mL. When [NO₂⁻] was < 0.5 μM, 10 mL of sample was added to
256 each headspace vial and the NaNO₂⁻ isotope standard N7373 was added as carrier to a final
257 amount of 5 nmol. Finally, 10 μmol of KNO₃⁻ was added to each sample to dilute the initial
258 ¹⁵NO₃⁻ tracer and samples were purged with ultra-high purity N₂ for 30 min. Following azide
259 conversion to N₂O, samples and standards (N23, N7373, and N10219; (Casciotti *et al.*, 2007)
260 were analyzed by IRMS and rates were calculated as described above.

261

262 2.3.4 Light inhibition experiments

263

264 Light inhibition experiments were conducted in Year 2 to test the effect of sunlight on
265 ammonia oxidation, nitrite oxidation, and nitrate reduction. These incubations were
266 conducted at the two shallowest incubation depths, approximating the 1% and 10% light

267 depths at Stns. 7, 9, and 11. For these experiments, one set of duplicate incubation bottles
268 for each rate type was incubated at ambient light and the other in the dark. Tracer addition,
269 subsampling, analysis, and rate calculations were as described above for each individual
270 rate type.

271

272 *2.3.5 Particle-associated ammonia oxidation rates*

273

274 Ammonia oxidation occurring in association with sinking particulate organic matter was
275 measured in both years ($n = 8$ experiments). Sinking particulate organic matter was captured
276 in drifting surface-tethered particle interceptor sediment traps ('PIT' traps) as described
277 previously (Haskell *et al.*, 2013). Each trap had 12 collection tubes that contained a funnel
278 and 50 mL centrifuge tube (BD Falcon) at the base of each tube. In Year 1, particle-
279 associated rates were measured at Stations 7 and 9 using material from a single collection
280 tube from traps deployed at 200 m depth. On recovery of the trap, the trapping solution (a
281 concentrated NaCl brine) was decanted and particulate matter was resuspended in 15 mL of
282 0.2 μm -filtered seawater obtained from 200 m depth at the respective station. 5 mL of this
283 particle slurry was distributed to each of three 160 mL glass serum vials. Each vial was filled
284 with additional filtered seawater to a volume of 100 mL and spiked with $^{15}\text{NH}_4\text{Cl}$ to a final
285 concentration of 100 nM $[\text{NH}_4^+]$. Three bottles containing only filtered seawater served as a
286 negative control for ammonia oxidation that was not particle-associated. Bottles were
287 sampled for $\delta^{15}\text{NO}_x$ analysis after 24 h as described above for water column ammonia
288 oxidation rates.

289

290 In Year 2, particle-associated rates were measured at Stations 1, 7, and 11 using particulate
291 material from traps deployed at both 100 m and 200 m depths. Due to concerns that the trap
292 brine fluid used in the prior year could be negatively impacting particle-associated microbial
293 communities, centrifuge tubes designated for collection of incubation particles contained only
294 filtered seawater as a trap solution. On recovery of the trap, the seawater in the centrifuge
295 collection tube was decanted to the conical portion of the tube and particles were
296 resuspended in 10 mL of filtered seawater from the particle collection depth. A cutoff 5 mL
297 pipette was used to distribute 3 mL of particle slurry into each of three 160 mL serum vials.
298 Each vial was filled with additional filtered seawater to a volume of 100 mL and spiked with
299 $^{15}\text{NH}_4\text{Cl}$ to a final concentration of 400-600 nM $[\text{NH}_4^+]$. Three bottles containing only filtered
300 seawater served as a negative control.

301

302 Particles were filtered at the conclusion of the experiment onto 0.2 μm Supor filters (Pall) for
303 DNA extraction and analysis, thus no material was available for mass determination. As
304 such, the mass of particulate carbon added to each incubation was estimated from the
305 average areal particulate carbon flux (Haskell *et al.*, 2013).

306

307

308 **2.4 Dissolved N_2O concentration and production rates**

309

310 *2.4.1 N_2O concentration*

311

312 Samples for $[\text{N}_2\text{O}]$ analysis at 24 depths per station were drawn directly from the rosette after
313 dissolved oxygen samples were collected but before other sample collection, using silicone
314 tubing directed into a 160 mL glass serum bottle. The tubing was placed at the bottom of the
315 serum bottle and water was allowed to overflow the bottle for approximately 30 seconds
316 (approximately 3 volumes of the sample bottle). The tubing was then slowly withdrawn, and 1
317 mL of water was removed from the bottle to allow for expansion of the liquid during storage.

318 The sample was preserved with the addition of 100 μL of saturated mercuric chloride
319 solution, then capped with a gray butyl stopper (MicroLiter Analytical, 20-0025) and sealed
320 with an aluminum crimp. Samples were stored at room temperature in the dark until analysis.

321
322 N_2O concentration measurements were performed on an IRMS using a custom-built
323 automated purge and trap system (McIlvin and Casciotti, 2010). Dissolved N_2O
324 concentrations were determined by comparison of mass/charge (m/z) = 44 peak area against
325 analyses of known amounts of N_2O (1-10 nmol) and the volume of sample analyzed ($153.8 \pm$
326 0.5 mL). N_2O saturation was calculated relative to water in equilibrium with the atmosphere
327 (Weiss and Price, 1980), assuming a 'modern' atmospheric concentration of 322 ppb, the
328 modern tropospheric concentration for the Southern Hemisphere at the time of the cruises
329 (2010-2011) (Combined N_2O data obtained from the NOAA/ESRL Global Monitoring Division,
330 American Samoa station: ftp://ftp.cmdl.noaa.gov/hats/n2o/combined/HATS_global_N2O.txt).
331 Standard deviations for $[\text{N}_2\text{O}]$ are based on analyses of replicate samples. A total of 605
332 concentration measurements are presented here. Although $\delta^{15}\text{N}_{\text{N}_2\text{O}}$, $\delta^{18}\text{O}_{\text{N}_2\text{O}}$ and isotopomers
333 of N_2O ('site preference') were determined in concert with the concentration measurement, a
334 full treatment of those data is outside the scope of the present manuscript.

335
336

337 2.4.2 N_2O production rates

338

339 Nitrous oxide production from ammonia oxidation was determined in incubations with added
340 $^{15}\text{NH}_4\text{Cl}$ at Stns. 1, 9, and 11 in both years. In Year 1, N_2O production rates were determined
341 at the same four depths as nitrification rates; in Year 2, N_2O production rates were
342 determined at three of the six depths where ammonia oxidation rates were also measured:
343 the primary nitrite maximum, just below the primary nitrite maximum, and the top of the
344 oxycline. Incubations were conducted in 160 mL glass serum vials capped with 20 mm
345 diameter Teflon-backed gray butyl septa (MicroLiter Analytical, 20-0040AS) and sealed with
346 aluminum crimps. Bottles were filled from the Niskin bottles using silicone tubing, allowing
347 approximately three volumes of sample water to overflow the bottle prior to collection. Six
348 serum bottles were filled to overflowing and sealed from each incubation depth, spiked with
349 ^{15}N tracer (100-200 nM $^{15}\text{NH}_4\text{Cl}$) using a plastic syringe, and incubated in temperature-
350 controlled chambers as above. Duplicate bottles were killed at timepoints of 0, 12, 24 h from
351 each incubation depth by the addition of 100 μL of saturated HgCl_2 . In Year 2, similar
352 procedures were followed except that experiments were conducted in triplicate and an
353 additional timepoint was added (36 h). N_2O isotope measurements were determined by
354 isotope ratio mass spectrometry and calibrated against pulses of N_2O reference gas
355 analyzed just prior to elution of each sample (McIlvin and Casciotti, 2010). The reference gas
356 has been calibrated against AIR ($\delta^{15}\text{N}$) and VSMOW ($\delta^{18}\text{O}$) reference scales by S. Toyoda
357 (Tokyo Institute of Technology) (McIlvin and Casciotti, 2010).

358

359 N_2O production rates from NH_4^+ ($R_{\text{N}_2\text{O}-\text{N}}$ in $\text{nmol N}_2\text{O-N d}^{-1}$) were calculated using the slope of
360 the timecourse $[\text{}^{45}\text{N}_2\text{O}]$ and $[\text{}^{46}\text{N}_2\text{O}]$, where F is the fraction of ^{15}N in the substrate (NH_4^+) pool:

361

$$R_{\text{N}_2\text{O}-\text{N}} = \frac{1}{F} \left(\frac{d[\text{}^{45}\text{N}_2\text{O}]}{dt} + 2 \frac{d[\text{}^{46}\text{N}_2\text{O}]}{dt} \times \frac{1}{F} \right)$$

362

363 This formulation follows prior work (Ji et al., 2015; Trimmer et al., 2016; Ji et al., 2018)
364 accounting for the production of singly and doubly labeled N_2O from NH_4^+ . The $1/F$ terms
365 account for production of unlabeled N_2O via the same pathways. The probability of $^{46}\text{N}_2\text{O}$

366 production is proportional to $1/F^2$, thus the extra factor of $1/F$ is needed in that term relative to
367 production of $^{45}\text{N}_2\text{O}$.

368

369 **2.5 Quantitative PCR (qPCR)**

370

371 Quantitative PCR (qPCR) assays were conducted using group-specific assays for the
372 thaumarchaeal ammonia monooxygenase subunit a (*amoA*) gene for the 'shallow' water
373 column ecotype A (WCA) and 'deep' water column ecotype B (WCB) (Mosier and Francis,
374 2011) with TaqMan Environmental Mastermix (Life Technologies) chemistry on a CFX96
375 qPCR machine (Bio-Rad, Inc., Hercules, CA) as described previously (Santoro *et al.*, 2017).
376 Detection limits for TaqMan assays were 1 copy mL^{-1} or better. All samples were run in
377 triplicate against a standard curve spanning approximately 10^1 - 10^5 templates, run in
378 duplicate. Plasmids containing cloned inserts of the target gene (TOPO pCR4 vector,
379 Invitrogen or pGem vector, Promega) were used as standards. Standards were linearized
380 with the restriction enzyme NotI or Scal (New England Biolabs), purified (DNeasy, Qiagen),
381 quantified by fluorometry (Quanti-T HS reagent, Invitrogen), and stored at -80°C . Fresh
382 standard dilutions were made from frozen stocks for each day of analysis. All qPCR runs
383 were setup using an epMotion 5075 automated liquid handling system (Eppendorf) to
384 minimize between-run variability. Ammonia oxidizing bacteria (AOB; Year 1 only) and
385 *Nitrospina*-like 16S rRNA genes were quantified using primers (Mincer *et al.*, 2007) and
386 protocols (Santoro *et al.*, 2010) described previously with SYBR Green chemistry. We
387 verified (in silico) that this assay captures recently-described uncultivated *Nitrospina* from low
388 oxygen waters (Sun *et al.*, 2019).

389

390

391 **3. Results**

392

393 **3.1 Hydrography and nutrient distributions**

394

395 *3.1.1 Temperature, oxygen, and chlorophyll*

396

397 There were strong east-west gradients in all hydrographic parameters along both the
398 northern and southern transects (Table S1, Fig. 1). On the southern transect along 20°S
399 (Stns. 1-5), sea surface temperature (SST) ranged from 20.6 to 23.4°C in 2010, with mixed
400 layer depths from 28-68 m. The northern transect along 10°S (Stns. 7-11) had higher SSTs
401 (23.8 – 26.5°C) and shallower mixed layer depths. In general SSTs were higher in 2011 (on
402 average 0.7 $^\circ\text{C}$ higher), particularly at Stn 7, where SST was 2.6°C higher.

403

404 We used an arbitrary definition of 10 $\mu\text{mol kg}^{-1}$ $[\text{O}_2]$ to define the boundaries of the ODZ for
405 between-station and between-year comparisons. The ODZ was thicker on the northern
406 transect, ranging from 205 m thick at Stn 7 to 539 m thick at Stn 9. On the southern transect,
407 an ODZ was only present at Stn 1. On the eastern edge of the cruise track, oxygen
408 concentrations were near the ~ 1 $\mu\text{mol kg}^{-1}$ detection limit of the SBE43 sensor at Stn 9, 11,
409 and 13. The ODZ was thicker in Year 2, but did not extend as far offshore. For example, the
410 ODZ at St 11 was 467 m thick in Year 1, but 662 m thick in year 2.

411

412 There were pronounced deep chlorophyll maxima (DCM) at all stations, as deep as 137 m at
413 Stn 5 (Table S1, Fig. 2). Chl *a* profiles at Station 11 contained a secondary Chl *a* maximum
414 within the ODZ (Fig. 2c). In both years, the northern transect along 10°S (Stn 7, 9, and 11)
415 was characterized by higher primary production, higher surface Chl *a*, and higher depth
416 integrated Chl *a* than the southern transect (Table S1).

417

418 3.1.2 $[NH_4^+]$ and $[NO_2^-]$

419

420 Ammonium concentrations displayed typical distributions for stratified water columns, with
421 low but occasionally detectable $[NH_4^+]$ in surface waters increasing to a subsurface maximum
422 just below the deep chlorophyll maximum, and concentrations below detection limits at
423 deeper depths (Fig. 2). Particularly elevated shallow $[NH_4^+]$ was observed at Stn 11 in both
424 years, where $[NH_4^+]$ reached concentrations of up to 660 nM in surface waters.

425 Concentrations within the deep ammonium maximum ranged from 13 nM at the offshore Stn
426 5, to 2 μ M at Stn 11. When $[NH_4^+]$ data from both years are plotted together against density,
427 the profiles are nearly identical (Fig. S1).

428

429 A primary nitrite maximum (PNM) was present at all stations just below the ammonium
430 maximum (Fig. 2), ranging in concentration from 0.38 μ M at Stn 5 (in year 1) to nearly 3 μ M
431 at Stn 11 (also in year 1). Coincident with detectable $[NH_4^+]$ in surface waters, measurable
432 NO_2^- was present in surface waters at Stn 7 and 9 in year 1 and Stns 7, 9, and 11 in year 2.
433 A deeper, secondary nitrite maximum (SNM) was detectable within the ODZ at Stns 1, 9, and
434 11 in 2010, ranging from 0.31 μ M at Stn 1 to 2.1 μ M at Stn 11. The ODZ did not extend as far
435 west in 2011, and an SNM was only present at Stn 11 and 13 in that year. As with $[NH_4^+]$,
436 when $[NO_2^-]$ data from both years are plotted against density, profiles are very similar (Fig.
437 S2) with the exception of a much larger PNM at Stn 11 in year 1 versus year 2 (3.0 μ M
438 versus 1.3 μ M).

439

440 Depth-integrated inventories of NH_4^+ and NO_2^- between the surface and 200 m were
441 correlated with one another (Fig. S3a; Spearman's $\rho = 0.82$, $p = 0.003$), and with depth-
442 integrated primary production ($\rho = 0.70$, $p = 0.02$), with the highest inventories of both at
443 the station with highest primary production (Stn 11).

444

445 3.2 Rate measurements

446

447 3.2.1 Ammonia oxidation and nitrite oxidation rates

448

449 In general, ammonia and nitrite oxidation rates were low to undetectable in the euphotic
450 zone, highest in a subsurface maximum just below the PNM, and decreased with depth. In
451 both years, rates of both processes were higher along 10°S than 20°S, and were highest in
452 the east, closer to the coast (Fig. 3). Given the higher density of sampling, we specifically
453 discuss here only the rates from year 2. Rates from both years are given in Table S2.

454

455 Ammonia oxidation was detectable in the deep euphotic zone at Stns 9, 11, and 13 in both
456 years, with rates of 0.9 – 5.8 $nmol L^{-1} d^{-1}$ (Fig. 3, Table S2). Mean ammonia oxidation rates
457 within the subsurface rate maximum ranged from $1.7 \pm 1.4 nmol L^{-1} d^{-1}$ at Stn 3 to 50.8 ± 20.0
458 $nmol L^{-1} d^{-1}$ at Stn 11. Nitrite oxidation rate profiles had a similar shape to the ammonia
459 oxidation rate profiles, however nitrite oxidation was more frequently detected in the euphotic
460 zone, with rates above detection limits at the 1% light depth at all stations except Stn 7.

461

462 There was a marked difference in magnitude between ammonia oxidation and nitrite
463 oxidation rates in both years, with nitrite oxidation rates being much greater at a given depth.
464 Nitrite oxidation rates within the subsurface maximum ranged from $15.0 \pm 0.3 nmol L^{-1} d^{-1}$ at
465 Stn 9 to $57.1 nmol L^{-1} d^{-1}$ at Stn 13. The largest offsets between ammonia oxidation and
466 nitrite oxidation occurred near the base of the euphotic zone and at the lowest oxygen

467 concentrations. At Stn 13, nitrite oxidation rates continued to increase with depth into the
468 ODZ, reaching rates of $65.0 \pm 0.4 \text{ nmol L}^{-1} \text{ d}^{-1}$ at 100 m.

469
470 To investigate the factors controlling nitrification rates in the upper water column, we
471 categorized rate samples as originating from the euphotic zone, PNM, or upper oxycline after
472 (Peng *et al.*, 2016). Neither ammonia oxidation nor nitrite oxidation rates were correlated with
473 substrate concentration ($[\text{NH}_4^+]$ or $[\text{NO}_2^-]$) or oxygen concentration (data not shown) within
474 these categories. We further compared depth-integrated nitrification rates in the upper
475 mesopelagic (to 300 m depth) with primary production in the overlying euphotic zone and
476 sinking particulate organic nitrogen (PON) flux from sediment traps for both years. Depth-
477 integrated ammonia oxidation rates in the mesopelagic were not correlated with depth-
478 integrated primary production in the overlying euphotic zone, either in individual years or
479 when data from both years are combined ($\rho = 0.50$, $p = 0.10$). Depth integrated ammonia
480 oxidation rates were, however, correlated with absolute sinking PON flux at 200 m ($\rho =$
481 0.82 , $p = 0.003$; Fig. S4).

482
483 Ammonia oxidation rates in deeper waters (1000 - 2000 m depth) were determined at a
484 subset of stations in both years ($n = 10$, Table 1). Rates were low but detectable at these
485 depths at all stations, and ranged from $0.10 \text{ nmol L}^{-1} \text{ d}^{-1}$ to $0.88 \text{ nmol L}^{-1} \text{ d}^{-1}$. In all cases,
486 ammonia oxidation rates were lower at the deepest depth at each station. At the only station
487 to include deep rate measurements in both years (Stn 7), rates were not different between
488 years (student's *t*-test, $p < 0.0001$).

489 490 3.3.2 Nitrate reduction rates

493 Rates of nitrate reduction to nitrite were highest in the upper euphotic zone, ranging from
494 averages of $366 \text{ nmol L}^{-1} \text{ d}^{-1}$ at Stn 13 to $109 \text{ nmol L}^{-1} \text{ d}^{-1}$ at Stn 11 (Table 2). Nitrate
495 reduction in the euphotic zone occurred at higher rates than either ammonia or nitrite
496 oxidation. Deeper in the euphotic zone, nitrate reduction to nitrite was below detection limits
497 at the 1% light depth (the PNM) and the upper oxycline, with the exception of the depth of the
498 PNM at Stn 13, where nitrate reduction was 9.7 nM d^{-1} . There was no relationship between
499 nitrate reduction rate and primary production at an individual depth, or with depth-integrated
500 primary production by station.

501 502 503 3.3.3 Light inhibition experiments

505 Rates of ammonia and nitrite oxidation were both higher in dark bottles compared to light
506 bottles at the 1% light depth at Stn 11 (Fig. 4a,b). We observed a slight increase in relatively
507 low nitrite oxidation rates in the light at both the 1% and 10% light depths at Stn 7 and 9, with
508 a significant difference at the 1% light depth at Stn 7. Nitrate reduction rates were always
509 higher in the light (Fig. 4c).

510 511 3.3.4 Particle-associated ammonia oxidation rates

513 Ammonia oxidation rates were below the detection limit in particle samples from both Stn 7
514 and Stn 11 in Year 1. Similarly, in Year 2, ammonia oxidation was below detection limits in 4
515 out of 6 incubations (Table S3). Low rates of ammonia oxidation were detected on particles
516 from the two most productive stations, Stn 1 from the 200 m trap depth ($0.09 \pm 0.1 \text{ nmol mg}^{-1}$
517 d^{-1}) and Stn 11 from the 200 m trap depth ($0.18 \pm 0.08 \text{ nmol mg}^{-1} \text{ d}^{-1}$).

518
519
520
521
522
523
524
525
526
527
528
529
530
531
532
533
534
535
536
537
538
539
540
541
542
543
544
545
546
547
548
549
550
551
552
553
554
555
556
557
558
559
560
561
562
563
564
565
566
567
568

3.4 Nitrous oxide distribution and production

3.4.1. *N₂O* distribution

General patterns in *N₂O* distribution were consistent between years, with higher *N₂O* concentrations on the northern transect at any given longitude, and relatively small horizontal gradients in *N₂O* concentration (Fig. 5a,b). *N₂O* was slightly supersaturated in surface waters at all stations in both years. Below the surface, the shapes of the *N₂O* profiles were qualitatively similar in both years, with some notable exceptions. Evidence of *N₂O* loss processes were present in profiles from Stn 9 and Stn 11 on the northern transect, particularly in Year 2, where *N₂O* concentrations decreased beginning at the upper oxycline to midwater minima of 18.7 nM (Stn 11) between 300 and 400 m depth forming a 'bite' in the *N₂O* profile. Deep water concentrations ($\sigma_T > 30$) were not different between years, with the exception of Stn 5, where deep *N₂O* concentrations were elevated by 2-3 nM in 2011 relative to 2010 (Fig. S5).

A notable feature in the *N₂O* dataset along 10°S was a sharp peak of very high *N₂O* concentration in the upper oxycline, even at the western extent of the cruise track, reaching 145 nM ($\sigma_T = 26.56$, depth = 90 m) at Stn 9 in Year 2 and 122 nM ($\sigma_T = 26.89$, depth = 150 m) at Stn 7 in Year 1. In both cases, these peaks in *N₂O* concentration occurred just above local minima in *N₂O*, and were higher than observed closer to the ODZ core.

3.4.2 Rates of *N₂O* production from ammonia oxidation

N₂O production from ammonia was determined using ¹⁵NH₄Cl tracer incubations at the three stations nearest the ODZ (Stns 1, 9, and 11; Table S4). In Year 1, *N₂O* production ranged from below the detection limit at Stn 1 to 83 pmol L⁻¹ d⁻¹ at Stn 11 at the top of the oxycline. In Year 2, *N₂O* production rates ranged from below detection limits to 156 pmol L⁻¹ d⁻¹ in the upper oxycline, again at Stn 11.

N₂O production rates were used in conjunction with measured ammonia oxidation rates (see above) to calculate the *N₂O* yield from ammonia oxidation (*N₂O*-N/mol NO₃⁻ produced, expressed as a percentage). *N₂O* yields ranged from 0.02% in the euphotic zone at station 1 to 2.93% at the top of the ODZ at station 11. The highest *N₂O* yields were observed in samples with < 10 μM O₂ (Fig. 6).

3.5 Abundance of nitrifying microorganisms

Profiles of *amoA* genes from ammonia-oxidizing archaea and 16S rRNA genes from *Nitrospina*-like nitrite-oxidizing bacteria were similar in shape to nitrification rate profiles: low in the euphotic zone, a maximum at the base of the euphotic zone, and decreasing with depth below (Fig. S6). Abundances of both archaeal *amoA* and *Nitrospina* 16S rRNA genes were slightly lower in Year 1 (Table S5), though sampling resolution was much lower in that year. Archaeal *amoA* abundance was highest at Stn 11, reaching concentrations of 2.0 x 10⁵ *amoA* genes mL⁻¹ at 200 m depth. Combining all samples from both years, total archaeal *amoA* genes were correlated with *Nitrospina*-like 16S rRNA genes and best described by an exponential relationship ($n = 54$, $R^2 = 0.81$, $p < 0.0001$ on log₁₀ transformed data, Fig. S7).

569

570 Particulate samples obtained from sediment traps in Year 2 were also screened for the
571 presence of nitrifying organisms ($n = 6$). Five of six samples were below detection limits for
572 archaeal *amoA*, and all samples were below detection limits for *Nitrospina*. The exception
573 was the 100 m trap from station 7, which contained 1550 *amoA* genes mg^{-1} particle (Table
574 S5).

575

576 Ecotype-specific qPCR assays were used to quantify the shallow (WCA) and deep (WCB)
577 clades of ammonia-oxidizing archaea for Year 2 samples. WCA-like *amoA* genes were more
578 abundant in samples shallower than 200 m, while WCB-like *amoA* genes were more
579 abundant below. The transition from a WCA-dominated community to a WCB-dominated
580 community was sharp, with the vast majority of samples containing >90% of one ecotype or
581 the other (Table S5).

582

583 There was no significant relationship between total *amoA* genes and ammonia oxidation
584 rates. There was, however, a positive correlation between WCA *amoA* genes and ammonia
585 oxidation rates ($R^2 = 0.61$, $p < 0.0001$; Fig. 7a). *Nitrospina*-like 16S rRNA genes were also
586 positively correlated with nitrite oxidation rates ($R^2 = 0.40$, $p < 0.001$; Fig. 7b).

587

588

589 4. Discussion

590

591 4.1 Nitrification in the context of upper ocean organic matter remineralization

592

593 Our data show the direct connection between sinking particulate organic nitrogen (PON) flux
594 and ammonia oxidation rates in the upper ocean. This relationship has been explored
595 previously by comparison of nitrification rate profiles and organic matter flux attenuation
596 profiles, which both display a power law relationship with depth (Martin *et al.*, 1987; Ward,
597 2008; Ward and Zafiriou, 1988). Previous work has found a close correspondence between
598 power law exponents (attenuation coefficients, or 'b' values) calculated from fitting a power
599 law function to both particulate organic carbon (POC) flux profiles and nitrification rates
600 (Newell *et al.*, 2011; Peng *et al.*, 2015; Smith *et al.*, 2015), though previous studies have not
601 been able to make contemporaneous measurements on the same cruise. Here, as
602 previously reported for the equatorial Pacific (Santoro *et al.*, 2017), we found a correlation
603 between direct measurements of PON flux attenuation and depth-integrated nitrification
604 rates, suggesting that even in oxygen poor regions of the ocean, the primary control on
605 depth-integrated nitrification rates is substrate supply delivered by sinking particulate matter.

606

607 Though there was a correlation between sinking PON flux and nitrification rates, we found
608 little evidence for nitrification occurring on particles either in ^{15}N -based rate measurements or
609 in molecular assays designed to target AOA and NOB. Particle-associated ammonia
610 oxidation rates were low to undetectable, AOA were detected in only one sediment trap
611 sample, and *Nitrospina*-like organisms not detected in any. This is consistent with previous
612 findings indicating that thaumarchaea are enriched in the free-living fraction of size-
613 fractionated metagenomes (Fuchsman *et al.*, 2017; Ganesh *et al.*, 2014). Thus, it appears
614 that sinking particles serve as sites of ammonification and/or urea release, but that the
615 nitrification process occurs among free-living microorganisms in the water column. As $[\text{NH}_4^+]$
616 is less than 10 nM at the depths of highest ammonia and nitrite oxidation rates (except at
617 Stn. 13), ammonium regeneration from particles and oxidation must be closely coupled
618 (Ploug and Bergkvist, 2015). Narrow zones of particle processing have been identified at
619 density interfaces in the water column, where slow particle sinking rates lead to zones of

620 intense remineralization (Prairie *et al.*, 2017). Interestingly, we find an intense zone of
621 nitrification just below the euphotic zone, which may indicate one such region (Fig. 3).

622
623 Depth-integrated nitrification rates were not correlated with primary production, yet we found
624 that the euphotic zone ammonium and nitrite inventories were linearly related to primary
625 production. While this general trend has been observed previously (Raimbault *et al.*, 2008;
626 Santoro *et al.*, 2013), this quantitative relationship between depth-integrated inventories has
627 only been reported once (Brzezinski, 1988) as extensive shipboard $[\text{NH}_4^+]$ profiles are
628 relatively rare. This observation provides support for the hypothesis that the source of NO_2^- in
629 the PNM originates from ammonia oxidation, as ammonia oxidation provides a direct link
630 between the inventories of NH_4^+ and NO_2^- . The factors limiting nitrite oxidation in the PNM
631 that allow such high accumulations of NO_2^- (here up to 3 μM) still remain to be elucidated. A
632 recent modeling study suggested that the depth distribution of $[\text{NH}_4^+]$ and $[\text{NO}_2^-]$ around the
633 PNM could be explained by differences in the cell sizes and energy yields of ammonia and
634 nitrite oxidizers, predicting an $[\text{NH}_4^+]:[\text{NO}_2^-]$ of about 1:10 at the PNM (Zakem *et al.*, 2018).
635 Here, we find $[\text{NH}_4^+]:[\text{NO}_2^-]$ at the PNM much lower, $\leq 1:100$, suggesting additional, poorly
636 understood biological or physical factors (such as grazing or mixing) that raise the effective
637 subsistence concentration of NO_2^- for NOB.

638
639 A somewhat surprising finding in our study was the relatively high $[\text{NH}_4^+]$ (up to 660 nM) and
640 $[\text{NO}_2^-]$ (160 nM) in surface waters. The ocean is the largest natural source of NH_3 to the
641 atmosphere (Johnson *et al.*, 2008; Paulot *et al.*, 2015); our data are consistent with global
642 biogeochemical models (Paulot *et al.*, 2015) indicating the ETSP is a large potential source
643 of NH_x to the atmosphere. High model-derived NH_x flux from this region has previously been
644 interpreted to derive from iron limitation, and contemporaneous measurements of iron
645 limitation on our cruises did find evidence for iron limitation of N_2 fixation (Dekaezemacker *et al.*,
646 2013) at the same locations where we observed high $[\text{NH}_4^+]$. An alternative explanation
647 (Paulot *et al.*, 2015) suggests that high surface water $[\text{NH}_4^+]$ originates from photolysis of
648 DON. In either case, ammonia oxidation rates were below detection in the upper euphotic
649 zone at these stations, which would allow NH_4^+ to accumulate. In contrast, rates of nitrite
650 oxidation in the upper euphotic zone are slightly higher in the light (Fig. 4), suggesting that
651 the NO_2^- supporting this process must originate from something other than ammonia
652 oxidation, such as nitrate reduction by phytoplankton or photolysis of NO_3^- (Zafiriou and True,
653 1979). Our results from the light-dark experiments support previous work showing that
654 ammonia oxidation rates are lower in the light (Horak *et al.*, 2018; Smith *et al.*, 2014a),
655 though our experimental design cannot resolve whether this effect is due to competition with
656 phytoplankton for NH_4^+ or direct photoinhibition.

657
658

659 **4.2 Apparent decoupling between ammonia and nitrite oxidation**

660
661 We frequently observed large differences between the magnitude of ammonia oxidation and
662 nitrite oxidation rates (Fig. 3). Large offsets between these two processes are unexpected in
663 oxic water columns, as the only source of NO_2^- to support nitrite oxidation should be from
664 ammonia oxidation, thus constraining the nitrite oxidation rate to the ammonia oxidation rate.
665 Yet, such offsets have been reported previously in coastal ODZs (Bristow *et al.*, 2017;
666 Buchwald *et al.*, 2015; Ganesh *et al.*, 2015; Kitinger *et al.*, 2020; Lipschultz *et al.*, 1990),
667 and the causes of such offsets are infrequently discussed. Here we explore several
668 hypotheses that could explain these observations.

669

670 If the observed rate differences are methodological artifacts, they could result from either an
671 underestimation of the ammonia oxidation rate or an overestimation of the nitrite oxidation
672 rate. An underestimation of ammonia oxidation could be due to isotope dilution of the added
673 $^{15}\text{NH}_4^+$ by newly produced NH_4^+ , as has been reported for ammonium uptake measurements
674 (Glibert *et al.*, 1982). If an underestimation of ammonia oxidation due to isotope dilution is the
675 cause, we would expect to see the biggest offsets between ammonia oxidation and nitrite
676 oxidation at the depths of the highest ammonia oxidation rates. We did observe a correlation
677 between the ammonia oxidation rate at a given depth and the magnitude of the ammonia
678 oxidation and nitrite oxidation rate difference at the same depth ($r = 0.51$, $p < 0.01$; Fig. S8a),
679 providing partial support for this idea. Another potential cause of underestimation of ammonia
680 oxidation rates is a greater sensitivity of ammonia-oxidizing organisms to bottle incubation
681 conditions than NOB.

682
683 The alternative explanation for the observed offset between ammonia oxidation and nitrite
684 oxidation is that we are overestimating the nitrite oxidation rate, either due to stimulation by
685 oxygen introduced in the handling process or substrate stimulation of NO_2^- limited organisms.
686 There is a very strong correlation between the ammonia and nitrite oxidation rate offset and
687 the magnitude of the nitrite oxidation rate ($r = 0.94$, $p < 0.0001$; Fig. S8b), suggesting that the
688 observed offsets are controlled primarily by variation in nitrite oxidation. While the largest
689 offset was observed at $1 \mu\text{mol kg}^{-1} \text{O}_2$, large offsets were also observed at $160 - 200 \mu\text{mol}$
690 $\text{kg}^{-1} \text{O}_2$, arguing against a role for O_2 stimulation in controlling the offset. Timecourse
691 measurements of $^{15}\text{N}/^{14}\text{N}$ in the tracer incubations were highly linear (data not shown),
692 perhaps providing evidence against oxygen contamination. Further, nitrite oxidation in ODZs
693 has been shown to have a half-saturation constant (K_m) of $< 1 \mu\text{M}$ for O_2 (Bristow *et al.*,
694 2016), below most of the *in situ* concentrations observed here. Given the extremely low $[\text{NO}_2^-]$
695 at most of the incubation depths, stimulation of nitrite oxidation by the addition of $^{15}\text{NO}_2^-$
696 tracer is certainly a possibility. K_m values for NO_2^- for marine NOB are few, but the data that
697 do exist indicate values in the $20\text{-}30 \mu\text{M}$ range (Jacob *et al.*, 2017).

698
699 A final but intriguing possibility is that the offsets between ammonia and nitrite oxidation rates
700 in bottle experiments are real and accurately reflect a stoichiometric decoupling of the two
701 processes in the water column. Nitrate reduction within anoxic zones in sinking aggregates
702 may provide an additional source of NO_2^- for nitrite oxidation in the water column. Modeling
703 suggests that nitrate reduction rates could be high even in oxic water columns (Bianchi *et al.*,
704 2018), and recent geochemical and metagenomic data suggest an enrichment of nitrate-
705 reducing activity in particle-associated over free-living environments (Fuchsman *et al.*, 2017;
706 Ganesh *et al.*, 2015). Unfortunately, the nitrate reduction rate measurements conducted as
707 part of this study were limited to the upper water column and cannot be used to answer this
708 question.

709 710 **4.3 Insights into nitrification from organismal distributions**

711
712 Our data suggest that specific clades of AOA contribute differentially to ammonia oxidation in
713 the water column. The abundance of the shallow ecotype of marine AOA (the 'WCA' clade),
714 which contains the cultivated AOA *Candidatus Nitrosopelagicus brevis* (Santoro *et al.*, 2015),
715 was strongly correlated with ammonia oxidation rates with a very similar slope to that found
716 by (Smith *et al.*, 2014b) in Monterey Bay (Fig. 7a).

717
718 There is a close, but non-linear, coupling of AOA and NOB in water column. The mean ratio
719 of NOB to AOA was 0.49 when samples containing < 10 genes mL^{-1} are removed. This is
720 much higher than recently reported for the Gulf of Mexico (Kitzinger *et al.*, 2020), but is

721 similar to the ratio of NOB:AOB reported for nitrifying sequencing batch reactors (Dytczak *et*
722 *al.*, 2008). It has been suggested that deviations from this ratio resulting in high NOB:AOB
723 ratios may result from coupling between denitrification and nitrification, as present in
724 activated granular sludge (Winkler *et al.*, 2015). In our data, however, deviations from this
725 ratio were not clearly tied to ambient oxygen concentration (Fig. S7). It should be noted that
726 the NOB:AOA ratio we calculate here does not account for other potential NOB, such as
727 *Nitrospira spp.* or *Nitrococcus spp.*, but *Nitrospina* have been shown to be the most abundant
728 both within and along the margins of other low oxygen regions in the Pacific (Beman *et al.*,
729 2013; Ganesh *et al.*, 2015; Sun *et al.*, 2019).

730

731 The qPCR data may also provide some insight into the offsets observed between ammonia
732 oxidation and nitrite oxidation – the correlation between nitrite oxidation rates and *Nitrospina*
733 gene copies suggests that the nitrite oxidation rates are accurate and reflect the abundance
734 of NOB in the water column, thus implying that the observed offsets between ammonia
735 oxidation and nitrite oxidation are real.

736

737 **4.4 Contribution of ammonia oxidation to N₂O distributions in the offshore ETSP**

738

739 In both years, N₂O production from NH₄⁺ was detectable from at least one depth at all stations
740 where measurements were made (i.e., Stns. 1, 9, and 11). Thus, despite arguments that
741 AOA are incapable of N₂O production, there is clear production of N₂O from ¹⁵NH₄⁺,
742 presumably carried out by AOA in these samples, consistent with previous marine
743 observations (Ji *et al.*, 2015; Ji *et al.*, 2018; Yoshida *et al.*, 1989). We observed both ⁴⁵N₂O
744 and ⁴⁶N₂O production in our incubations, indicating production of both singly and doubly
745 labeled N₂O from NH₄⁺. At most depths, production of singly labeled N₂O exceeded
746 production of doubly labeled N₂O. Due to the high atom% ¹⁵N labeling of the NH₄⁺ pool,
747 singly labeled N₂O is most likely to occur through a hybrid mechanism, while the doubly
748 labeled N₂O could arise from a NH₄⁺ oxidation pathway. Whether enzymatic or not, this
749 strongly suggests that at least some N₂O production is occurring within the cell envelope of
750 ammonia oxidizers and results from a combination of pathways as originally proposed for the
751 AOA (Santoro *et al.*, 2011), and consistent with recent laboratory experiments (Jung *et al.*,
752 2019).

753

754 The N₂O yield from nitrification is an important parameter for modeling N₂O production in the
755 ocean, and is a large source of uncertainty in global biogeochemical models. N₂O yield from
756 nitrification has been estimated from geochemical measurements based on the relationship
757 between N₂O supersaturation and AOU (Nevison *et al.*, 2003). This relationship breaks
758 down, however, in low oxygen regions of the ocean due to the combined and potentially
759 opposing effects of nitrification and denitrification at low O₂, where there may be increased
760 N₂O yield from nitrification, as well as denitrification, but also potential consumption of N₂O
761 due to microbial denitrification. Experimental data are needed to separate the contributions of
762 these processes in order to effectively model microbial N₂O production in low oxygen regions
763 (Martinez-Rey *et al.*, 2015; Suntharalingam *et al.*, 2000). We report here N₂O yields (mol
764 N₂O-N/mol NO₃⁻) from nitrification of 0.003 – 2.93%, which are similar to, but somewhat lower
765 than, N₂O yields from ammonia oxidation in the ETSP ODZ core (Ji *et al.*, 2015; Ji *et al.*,
766 2018), where N₂O yields as high as 3.14% were reported. Our values are about 50 times
767 lower than those reported in classic culture experiments with ammonia-oxidizing bacteria
768 grown at high density with high substrate concentrations (Goreau *et al.*, 1980), but very
769 similar to results from more field-relevant conditions 0.051% and 0.055% (220 and 22 μM O₂)
770 for *Nitrosomonas marina* (Frame and Casciotti, 2010) and marine ammonia-oxidizing
771 archaea (0.004 – 0.11%)(Qin *et al.*, 2017; Santoro *et al.*, 2011).

772

773 Nevison (Nevison *et al.*, 2003) modeled N₂O yield as a function of oxygen using available
774 laboratory culture data at the time (Goreau *et al.*, 1980) with the simple function:

775

$$776 \quad \% \text{ N}_2\text{O yield (mol N}_2\text{O/mol NO}_3^- * 100) = a_1 / \text{O}_2 + a_2 \quad [1]$$

777

778 with best-fit values of $a_1 = 0.20$ and $a_2 = -0.0004$. Note that (Nevison *et al.*, 2003) expressed
779 N₂O yield as mol N₂O/mol NO₃⁻ (*not* mol N₂O-N as reported above for culture comparisons)
780 and O₂ in units of μmol L⁻¹, thus the coefficients a_1 and a_2 in Eq. [1] apply to yields and O₂
781 expressed in those units. Recently, Ji and coworkers (Ji *et al.*, 2018) updated this
782 relationship using N₂O yields from ¹⁵N tracer experiments in the core ETNP and ETSP ODZs.
783 We combined our field data together with the data of Ji *et al.* 2018 and recent data from
784 cultures of marine ammonia-oxidizing archaea grown under different oxygen conditions (Qin
785 *et al.*, 2017, Santoro, *unpublished*) to further refine this relationship. Fitting Eq. 1 (again, with
786 units of mol N₂O/mol NO₃⁻) to those data, we obtain coefficients (\pm 95% CI) of $a_1 = 0.11 \pm$
787 0.05 and $a_2 = 0.077 \pm 0.07$ (Fig. 6). It should be noted, however, that there is considerable
788 scatter in the field data at low [O₂], and that a major assumption of least-squares fitting
789 methods is that there is no error in the independent variable (*i.e.*, [O₂]). Given the imprecision
790 of standard oxygen electrodes at low [O₂], we suggest that future experiments should focus
791 on N₂O yield measurements in the critical window of O₂ <10 μmol kg⁻¹, and conduct
792 continuous O₂ monitoring throughout the incubation rather than relying on CTD measured O₂
793 values as we (and others) have done. Our data appear to support previous field (Bristow *et al.*,
794 2016; Ji *et al.*, 2015) and laboratory (Qin *et al.*, 2017) experiments that suggest
795 nitrification can proceed at concentrations of O₂ near 1 μmol L⁻¹, lower than the 2-4 μmol L⁻¹
796 used in previous modeling efforts (Babbin *et al.*, 2015).

797

798 **4.5 Source of N₂O in offshore waters and implications for atmospheric N₂O flux**

799

800 We found that N₂O accumulates to high concentrations (>140 nM) in the ETSP outside of the
801 ODZ core. In the ODZ core, previous measurements attributed high rates of N₂O production
802 to both nitrification (Ji *et al.*, 2015; Peng *et al.*, 2016) and denitrification (Babbin *et al.*, 2015;
803 Farias *et al.*, 2009). N₂O maxima above the ODZ over the continental shelf (70.70°W) in the
804 ETSP were 80-86 nM (Farias *et al.*, 2009; Peng *et al.*, 2016); here, we measured N₂O
805 concentrations up to 122 nM as far offshore as 100° W (Stn 7) and 137 nM at 90° W (Stn 9),
806 concentrations typically associated with highly productive coastal waters and episodic
807 upwelling events (Arevalo-Martínez *et al.*, 2015; Bourbonnais *et al.*, 2017; Farías *et al.*,
808 2015). The steep N₂O gradients at the base of the mixed layer may also contribute to higher
809 atmospheric N₂O fluxes than previously estimated. Indeed, based on a range of air-sea gas
810 exchange parameterizations, atmospheric N₂O fluxes averaged along 10°S are estimated at
811 1.30 – 1.71 μmol m⁻² d⁻¹ (Table 3), 1.7 – 2.2 times higher than previously estimated in this
812 offshore region (Nevison *et al.*, 1995), but much lower than atmospheric fluxes measured
813 closer to the Peruvian and Chilean coast (12.7 – 30.7 μmol m⁻² d⁻¹ (Farias *et al.*, 2009), 459 –
814 1825 μmol m⁻² d⁻¹ (Arevalo-Martínez *et al.*, 2015)).

815

816 The source of the high N₂O at the base of the euphotic zone at 90° and 100° W is puzzling. It
817 is possible that the observed N₂O is due to lateral advection from the ODZ, though N₂O
818 concentrations further east at 82.5° W are lower (< 95 nM at the N₂O max at Stn 11), and
819 elevated N₂O concentrations are not associated with T-S anomalies (data not shown). Using
820 measured ammonia oxidation rates and the N₂O yield relationship derived above, we
821 estimate an N₂O production rate from ammonia oxidation of 0.08 nmol L⁻¹ d⁻¹ at the depth of
822 the N₂O maximum, and 0.12 nmol L⁻¹ d⁻¹ at the ammonia oxidation rate maximum, leading to

823 a residence time of over three years if ammonia oxidation is the only source of N₂O.
824 Assuming a conservative vertical diffusivity of 0.7 cm² s⁻¹ (Yeung *et al.*, 2015), the timescale
825 for diffusion over the upper 100 m of the water column is on the order of 4.5 years. Thus, it is
826 possible that these high concentrations result from a low but constant input of N₂O from
827 nitrification that is not quickly removed by physical processes. Given the potential for
828 reductive NO₂⁻ production suggested by our tracer experiments, there is also the possibility
829 of reductive N₂O production from microbial denitrification. Further investigation of physical
830 transport of N₂O from the ODZs combined with isotopic analysis of the N₂O in these offshore
831 waters should improve our understanding of the processes contributing to the observed N₂O
832 distributions.

833

834 **5. Conclusions**

835

836 Combining measures of surface primary production, particle export, and subsurface nitrogen
837 transformations reinforced the close connections between the mesopelagic nitrogen cycle
838 and euphotic zone processes. Nitrogen incorporated into biomass during primary production
839 sets the amount of particulate organic nitrogen available for remineralization in the lower
840 euphotic zone, controlling the inventories of both [NH₄⁺] and [NO₂⁻] that accumulate there.
841 Sinking particulate nitrogen flux exiting the euphotic zone, in turn, controls substrate
842 availability to the mesopelagic nitrifying community below. Together, our molecular and
843 geochemical data point to a dynamic nitrogen cycle in low oxygen areas of the ocean
844 offshore of those typically investigated in ODZ studies, with the potential for previously
845 unrecognized coupling of oxidative and reductive processes and greenhouse gas production.
846 We provide additional data to support the growing body of evidence that ammonia oxidation
847 in the ocean is directly linked to N₂O production. Our results highlight the need for additional
848 refinement of the nitrification-N₂O yield parameterization and for higher resolution
849 measurements of N₂O to resolve transport of N₂O both into and out of coastal ODZs.

850

851 **6. Acknowledgments and Data Availability Statement**

852

853 We thank the captains and crew of both the R/V *Atlantis* and R/V *Melville* for their invaluable
854 help during the cruises. Technical support from Troy Gunderson, Matt Tiahlo, Nick Rollins,
855 Matt McIlvin, and Matt Forbes was critical to the data reported here. Scientific discussions
856 with Masha Prokopenko, William Haskell, Nicholas Nidzieko, Simon Yang and Bonnie Chang
857 greatly improved the manuscript, as did manuscript comments from Barbara Bayer. Funding
858 for the cruises was provided by United States National Science Foundation awards OCE-
859 0850905 to ANK, DGC, and WMB; OCE-0961098 to KLC. Additional support for AES was
860 provided through a Woods Hole Oceanographic Institution Postdoctoral Scholar Fellowship
861 and a Sloan Foundation Early Career Award in Ocean Sciences. All datasets reported in this
862 manuscript have been deposited in the United States Biological and Chemical
863 Oceanography Data Management Office repository in association with project number
864 555516 (<https://www.bco-dmo.org/project/555516>). [Author note: BCO-DMO currently has an
865 ~8-10 week processing time. Datasets were submitted on 27 May 2020.]

866

867

868

869 **Table List**

870

871 Table 1. Deep ammonia oxidation rates

872 Table 2. Nitrate reduction rates

873 Table 3. Atmospheric N₂O flux

874

875

876 **Figure List**

877

878 Fig. 1a,b. Map of the cruise track over WOA oxygen data

879 Fig. 2a-f. Profiles of NH₄⁺, NO₂⁻, Chl a from 2011

880 Fig. 3 Ammonia oxidation and nitrite oxidation rate profiles

881 Fig. 4 Light/dark rate experiments

882 Fig. 5 N₂O concentration profiles

883 Fig. 6 N₂O yield as a function of oxygen

884 Fig. 7 Nitrification rates versus gene abundance

885

886

887 **Supplemental Table List**

888

889 Tabel S1. Physical parameters

890 Table S2. Ammonia oxidation and nitrite oxidation rates

891 Table S3. Particle-associated ammonia oxidation rates and qPCR data

892 Table S4. N₂O production rates

893 Table S5. qPCR data

894

895 **Supplemental Figure List**

896

897 Fig. S1. [NH₄⁺] from both years against density (six panel)

898 Fig. S2 [NO₂⁻] from both years against density (six panel)

899 Fig. S3 Depth-integrated NO₂⁻ versus NH₄⁺; PP versus NH₄⁺ (two panel)

900 Fig. S4 Ammonia oxidation vs. PON flux

901 Fig. S5 N₂O 6 panel with 2011 plotted over 2010

902 Fig. S6 qPCR profile six panel

903 Fig. S7 AOA vs. NOB with oxygen colorscale

904 Fig. S8 NH₄-NO₂ ox offset versus oxygen and NO₂ rate.

905

906

907 **Tables**

908

909 **Table 1.** Ammonia oxidation rates measured using $^{15}\text{NH}_4^+$ in deep waters of the Eastern
 910 Tropical South Pacific.

Year	Station	Depth (m)	Rate (nM d ⁻¹)	SE (nM d-1)
2010	5	1000	0.55	0.04
		2000	0.10	0.01
	7	1000	0.88	0.07
		2000	0.14	0.02
	9	1000	0.79	0.53
		2000	0.20	0.02
2011	7	1000	0.58	0.44
		2000	0.12	0.001
	13	1000	0.55	0.02
		1500	0.19	0.07

911

912 **Table 2.** Rates of nitrate (NO_3^-) reduction to nitrite (NO_2^-) measured using $^{15}\text{NO}_3^-$ tracer
 913 additions on the 2011 cruise. (BDL = below detection limit)

Station	Depth (m)	NO_3^- reduction rate (nM d ⁻¹)	SE rate (nM d ⁻¹)
7	30	261.2	63.5
7	85	0.1	0.0
7	140	BDL	
9	30	166.3	60.4
9	55	BDL	
9	80	0.0	0.0
11	14	108.8	49.6
11	55	1.5	0.2
11	70	BDL	
13	20	125.0	0.2
13	40	9.6	0.2
13	60	366.1	21.6

914

915

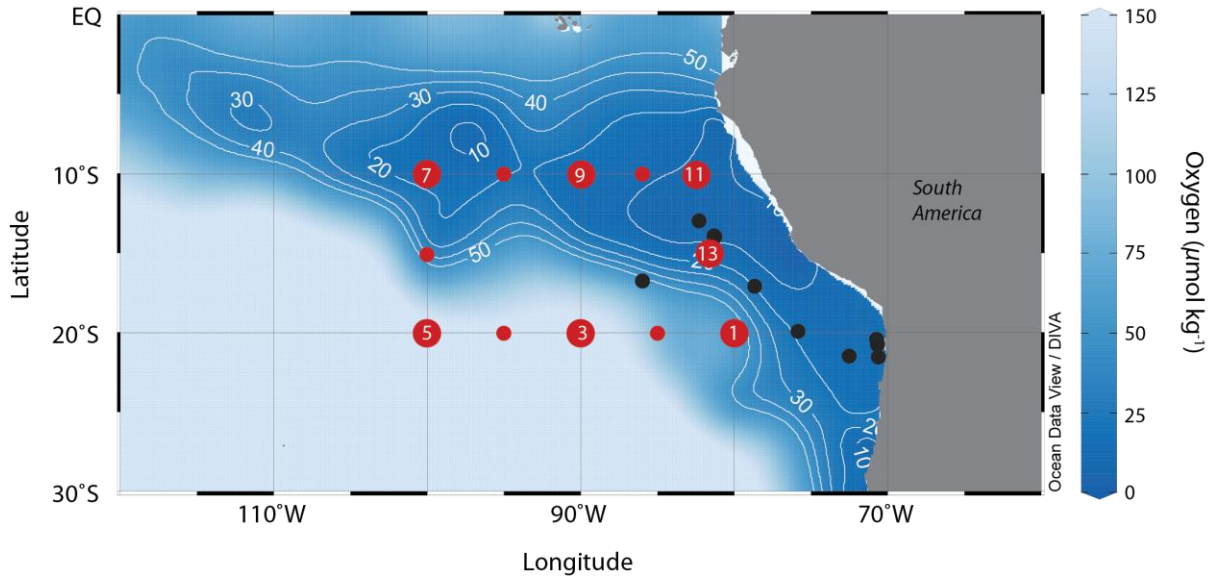
916

917 **Table 3.** Sea-to-air fluxes of N₂O in the Eastern Tropical South Pacific using data from the
 918 2010 cruise. Fluxes were determined using gas transfer velocities calculated using both
 919 wind-speed based parameterizations (Ho *et al.*, 2006; Wanninkhof, 1992) and mixed-layer
 920 ²²²Rn deficits, all as reported in (Yeung *et al.*, 2015).

Station	Mixed layer excess N ₂ O (μmol m ⁻³)	Atmospheric N ₂ O flux (μmol m ⁻² d ⁻¹)		
		Wind-W92	Wind-H06	²²² Rn-deficit
1	0.438	0.96	0.79	0.66
3	0.148	0.44	0.36	0.34
5	0.037	0.15	0.12	0.04
	0.037	0.13	0.11	0.09
7	0.490	1.67	1.37	1.32
	0.490	1.81	1.52	1.52
9	0.161	0.58	0.47	0.45
11	1.07	2.78	2.25	1.93
10°S transect average		1.71 ± 0.90	1.40 ± 0.73	1.30 ± 0.62
20°S transect average		0.42 ± 0.39	0.34 ± 0.32	0.28 ± 0.28

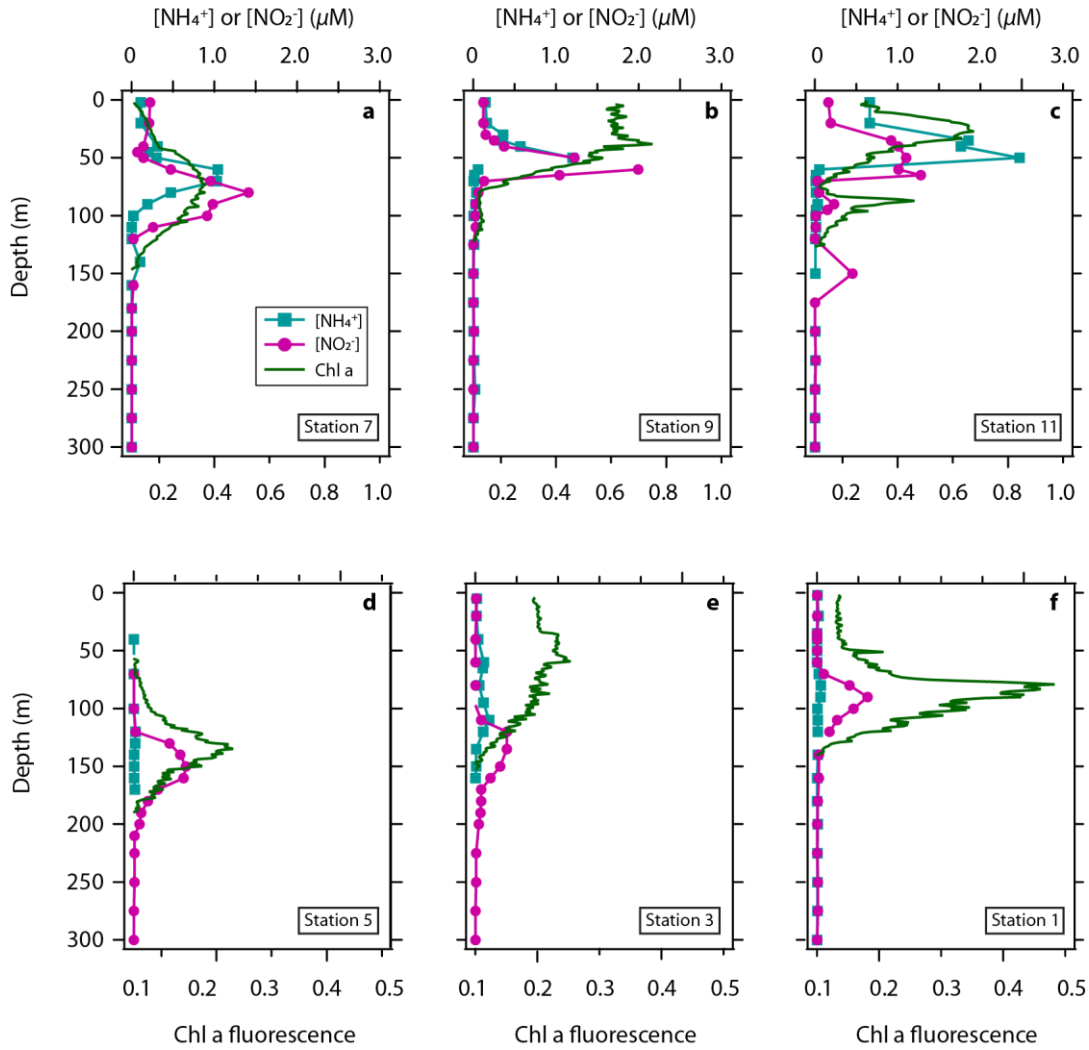
921
 922
 923
 924
 925

926 **Figures**
927
928



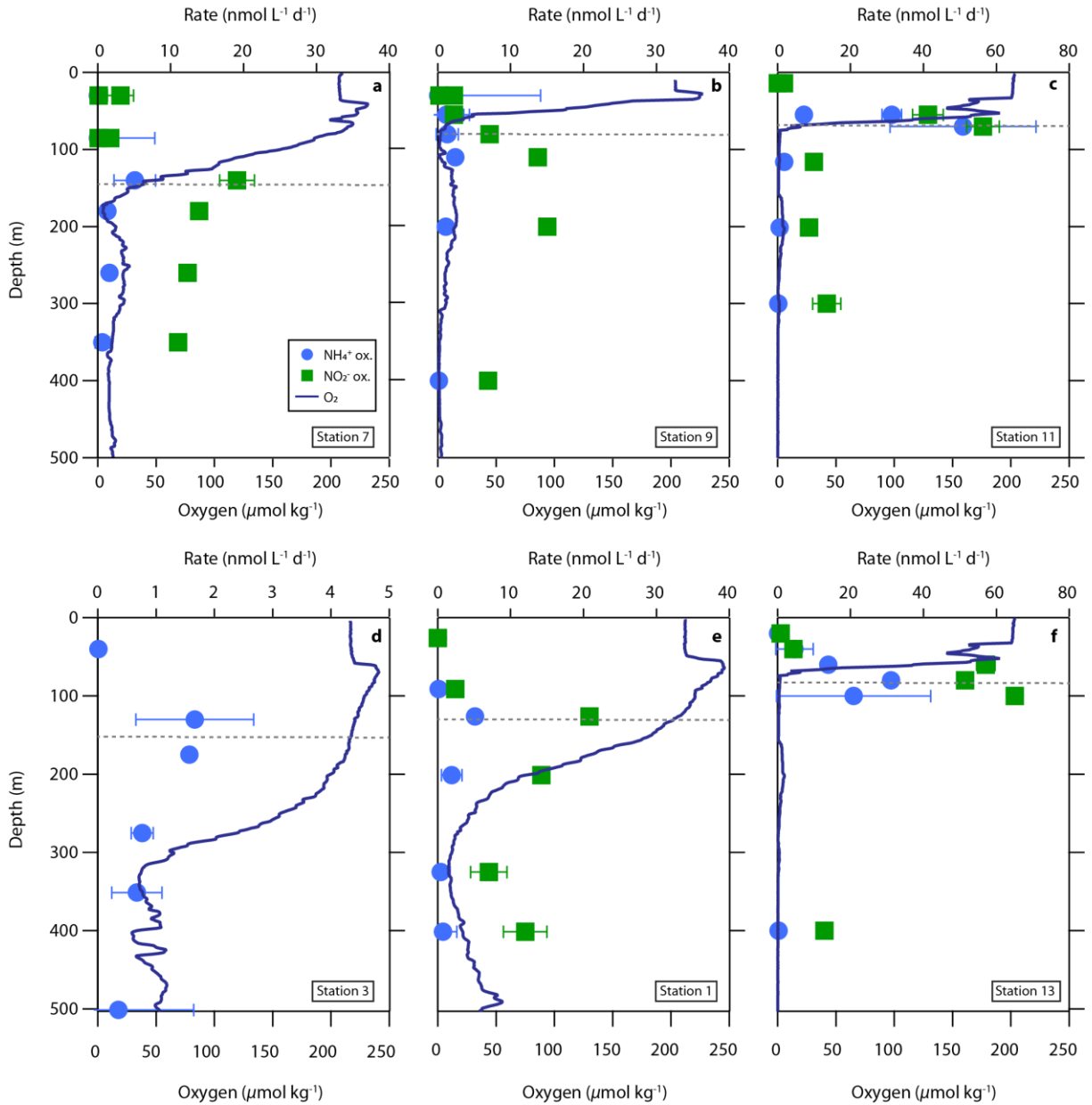
929
930
931
932
933
934
935
936
937
938
939
940

Figure 1. Map of the cruise track overlaid on dissolved oxygen concentration at the 200 m isobath (shown in both colorscale and contours). Large red dots indicate process study stations where rate measurements were conducted for the present study. Black dots indicate cruise track from (Ji *et al.*, 2015) and (Peng *et al.*, 2016). Oxygen data are monthly climatological means for March (1955-2012) from the World Ocean Atlas 1.00 degree gridded data product plotted in Ocean Data View v. 4.7.3 using the DIVA gridding algorithm with default settings.



941
 942
 943
 944
 945
 946
 947

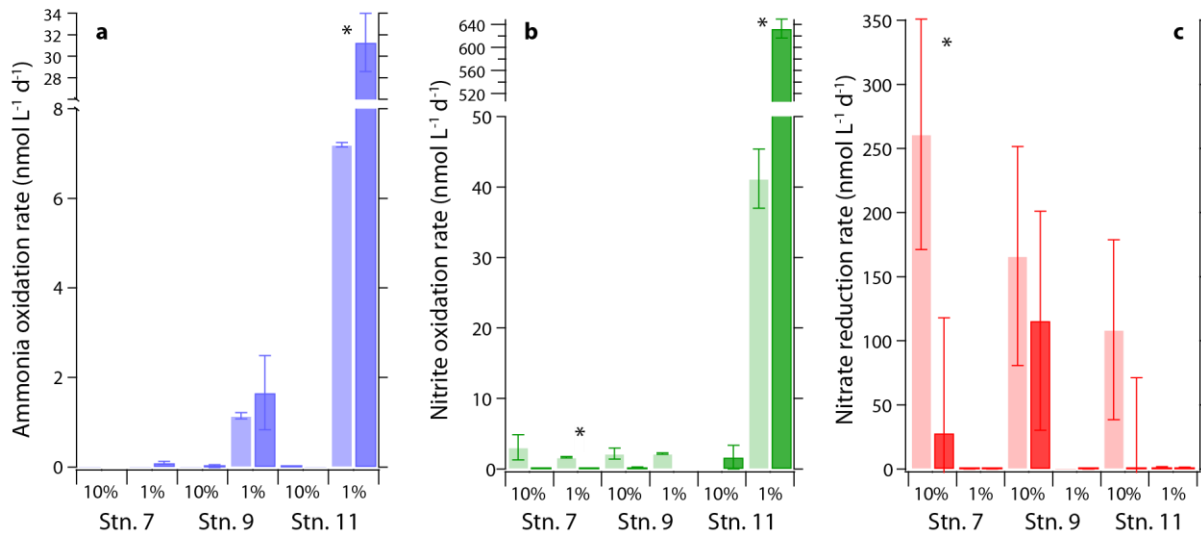
Figure 2. Profiles of ammonium ($[\text{NH}_4^+]$), nitrite ($[\text{NO}_2^-]$), and chlorophyll a fluorescence (Chl a) in the upper water column for the 2011 cruise along 10°S: (a) Stn 7, (b) Stn 9, (c) Stn11; and 20°S: (d) Stn 5, (e) Stn 3 (f) Stn1. Note the change in fluorescence scale between rows.



948
 949
 950
 951
 952
 953
 954
 955
 956

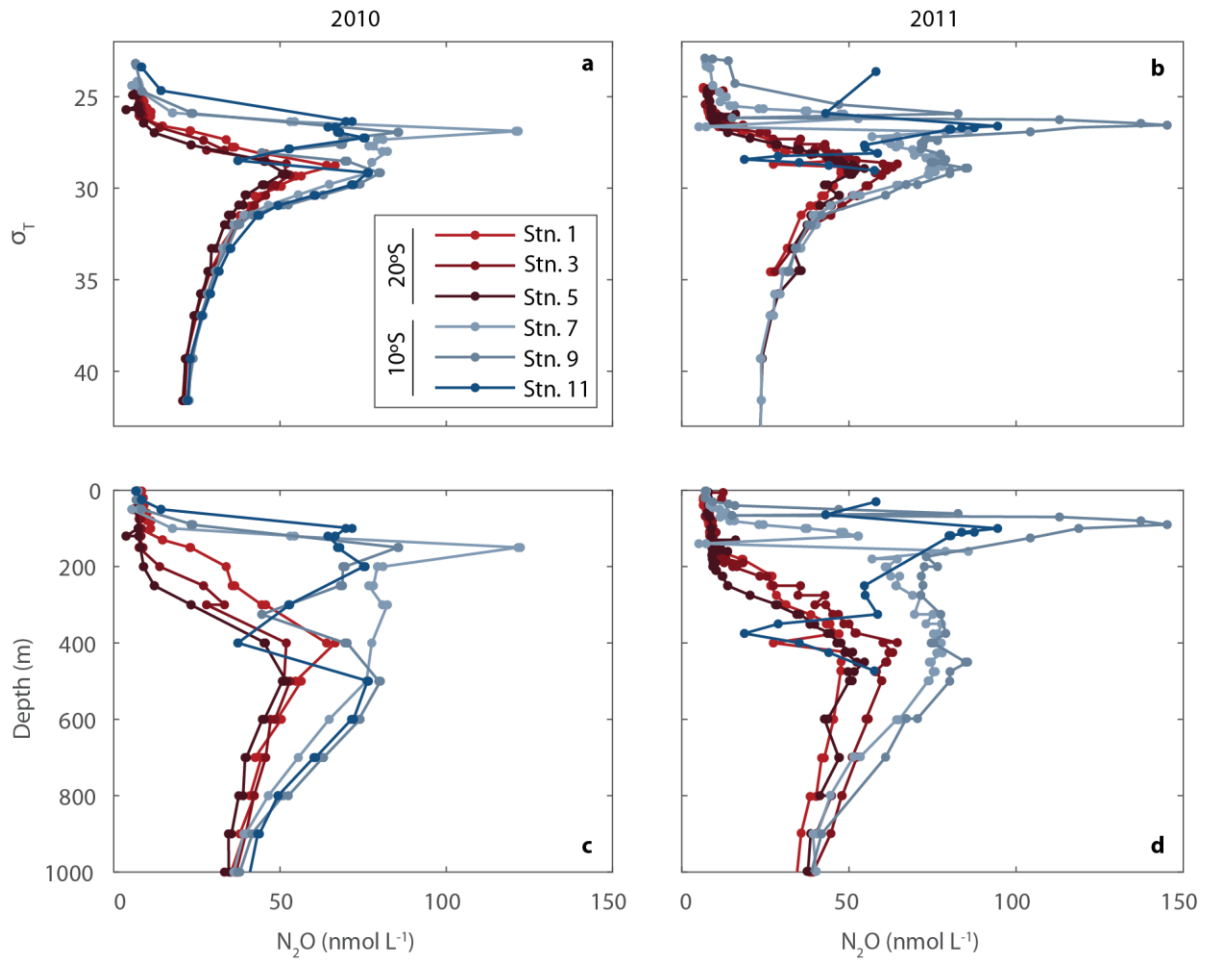
Figure 3. Measured nitrite oxidation rates exceed ammonia oxidation rates in the offshore ETSP. Ammonia oxidation rate (NH_4^+ ox., blue circles), nitrite oxidation rate (NO_2^- ox., green squares), and dissolved oxygen (dark blue line) along 10°S : (a) Stn 7, (b) Stn 9, (c) Stn11; and 20°S : (d) Stn 3, (e) Stn 1 (f) Stn13. Depth of the euphotic zone is indicated by the dashed line, calculated as 10% of the chlorophyll fluorescence maximum after correcting for sensor background (Owens *et al.*, 2015). Note panel order differs from Fig. 2.

957



958
959
960
961
962
963
964
965
966
967

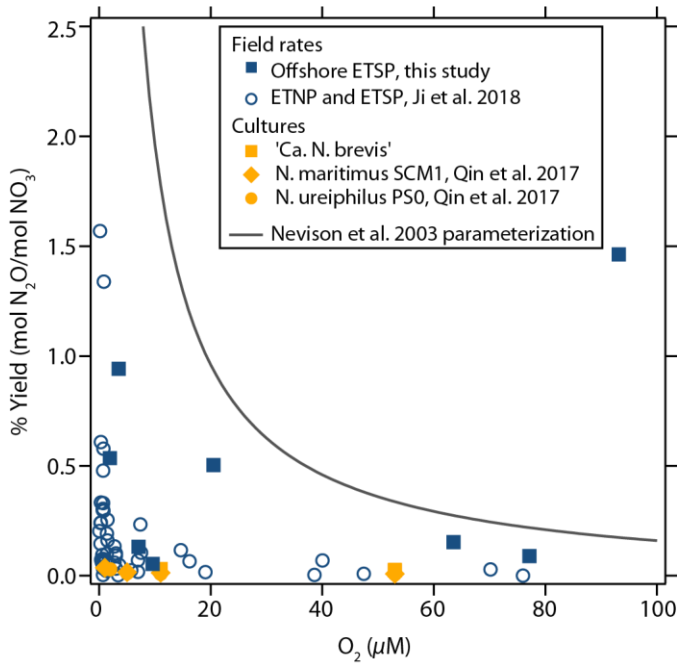
Figure 4. Ammonia and nitrite oxidation rates are higher in the dark. Rates of (a) ammonia oxidation, (b) nitrite oxidation, and (c) nitrate reduction measured in light (light bars) and dark (dark bars) incubations at Stns. 7, 9, and 11 during the 2011 cruise. Incubations were conducted with water collected from the depth of 10% surface irradiance and 1% surface irradiance at each station. Significant differences between the light and dark bottles at $p < 0.05$ are indicated with an asterisk.



968
 969
 970
 971
 972
 973
 974
 975

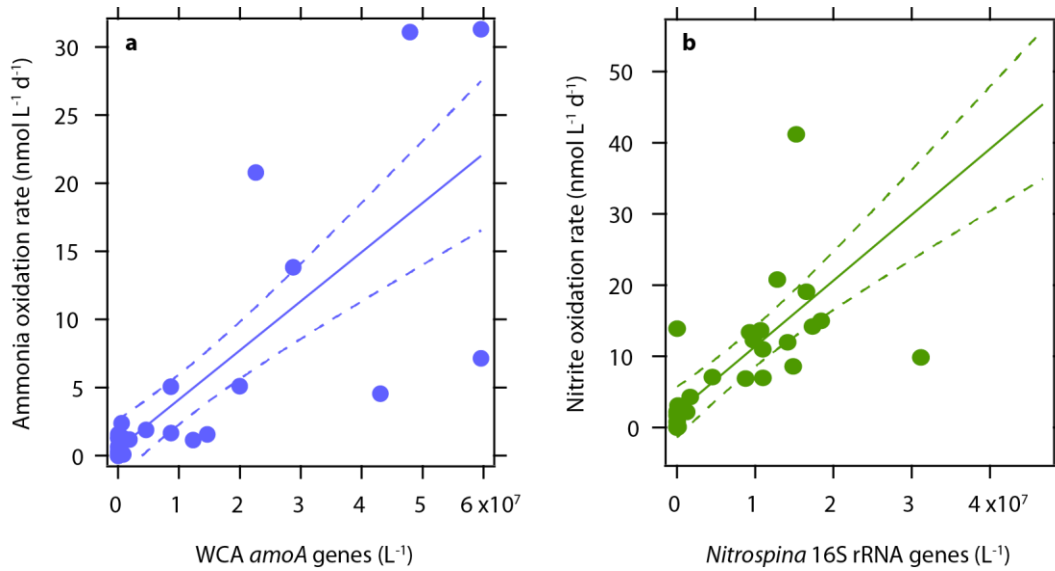
Figure 5. Nitrous oxide (N_2O) concentrations in the water column of the offshore ETSP. Data are shown plotted against density (σ_T , panels **a**, **b**) and depth (panels **c**, **d**) in Year 1 (2010, left column) and Year 2 (2011, right column).

976



977
978
979
980
981
982
983
984
985
986
987
988
989

Figure 6. Nitrous oxide (N_2O) yield from ammonia oxidation in low oxygen water columns and cultures of ammonia-oxidizing archaea (orange symbols). The black line is the relationship fit by (Nevison *et al.*, 2003) to the culture data of (Goreau *et al.*, 1980) from ammonia-oxidizing bacteria. Consistent with other recent studies (Ji *et al.*, 2015; Ji *et al.*, 2018), we find a considerably lower instantaneous yield. Fitting Eq. [1] gives $a_1 = 0.11 \pm 0.05$ and $a_2 = 0.077 \pm 0.07$ (curve not shown); note that percent yield data are plotted here as mol $\text{N}_2\text{O}/\text{mol NO}_3^-$ and O_2 in units of $\mu\text{mol L}^{-1}$ for consistency with (Nevison *et al.*, 2003). Samples with $\text{O}_2 < 0.05 \mu\text{mol L}^{-1}$ were removed for fitting.



990
 991
 992
 993
 994
 995
 996
 997
 998

Figure 7. Abundance of nitrifying organisms is correlated with the reactions they catalyze. (a) Ammonia oxidation rate versus thaumarchaeal *amoA* gene abundance from the water column A (WCA) ecotype (slope = 3.61×10^{-7} , $R^2 = 0.61$, $p < 0.0001$) and (b) nitrite oxidation versus *Nitrospina*-like 16S rRNA gene abundance (slope = 6.89×10^{-7} , $R^2 = 0.40$, $p < 0.001$).

999 **References**

1000
1001
1002
1003
1004
1005
1006
1007
1008
1009
1010
1011
1012
1013
1014
1015
1016
1017
1018
1019
1020
1021
1022
1023
1024
1025
1026
1027
1028
1029
1030
1031
1032
1033
1034
1035
1036
1037
1038
1039
1040
1041
1042
1043

Arevalo-Martínez, D. L., A. Kock, C. Löscher, R. A. Schmitz, and H. W. Bange (2015), Massive nitrous oxide emissions from the tropical South Pacific Ocean, *Nat Geosci*, 8(7), 530.

Babbin, A. R., D. Bianchi, A. Jayakumar, and B. B. Ward (2015), Rapid nitrous oxide cycling in the suboxic ocean, *Science*, 348(6239), 1127-1129.

Beman, J. M., J. L. Shih, and B. N. Popp (2013), Nitrite oxidation in the upper water column and oxygen minimum zone of the eastern tropical North Pacific Ocean, *ISME J*, 7(11), 2192-2205.

Berelson, W., W. Haskell, M. Prokopenko, A. Knapp, D. Hammond, N. Rollins, and D. Capone (2015), Biogenic particle flux and benthic remineralization in The Eastern Tropical South Pacific, *Deep Sea Res. I*, 99, 23-34.

Bianchi, D., J. P. Dunne, J. L. Sarmiento, and E. D. Galbraith (2012), Data - based estimates of suboxia, denitrification, and N₂O production in the ocean and their sensitivities to dissolved O₂, *Global Biogeochemical Cycles*, 26(2).

Bianchi, D., T. S. Weber, R. Kiko, and C. Deutsch (2018), Global niche of marine anaerobic metabolisms expanded by particle microenvironments, *Nat Geosci*, 11(4), 263.

Bourbonnais, A., M. A. Altabet, C. N. Charoenpong, J. Larkum, H. Hu, H. W. Bange, and L. Stramma (2015), N - loss isotope effects in the Peru oxygen minimum zone studied using a mesoscale eddy as a natural tracer experiment, *Global Biogeochemical Cycles*, 29(6), 793-811.

Bourbonnais, A., R. T. Letscher, H. W. Bange, V. Echevin, J. Larkum, J. Mohn, N. Yoshida, and M. A. Altabet (2017), N₂O production and consumption from stable isotopic and concentration data in the Peruvian coastal upwelling system, *Global Biogeochemical Cycles*, 31(4), 678-698.

Braman, R. S., and S. A. Hendrix (1989), Nanogram nitrite and nitrate determination in environmental and biological materials by vanadium (III) reduction with chemiluminescence detection, *Anal. Chem.*, 61(24), 2715-2718.

Bristow, L. A., T. Dalsgaard, L. Tian, D. B. Mills, A. D. Bertagnolli, J. J. Wright, S. J. Hallam, O. Ulloa, D. E. Canfield, and N. P. Revsbech (2016), Ammonium and nitrite oxidation at nanomolar oxygen concentrations in oxygen minimum zone waters, *Proceedings of the National Academy of Sciences*, 113(38), 10601-10606.

Bristow, L. A., C. M. Callbeck, M. Larsen, M. A. Altabet, J. Dekaezemacker, M. Forth, M. Gauns, R. N. Glud, M. M. Kuypers, and G. Lavik (2017), N₂ production rates limited by nitrite availability in the Bay of Bengal oxygen minimum zone, *Nat Geosci*, 10(1), 24.

Brzezinski, M. A. (1988), Vertical-Distribution of Ammonium in Stratified Oligotrophic Waters, *Limnol. Oceanogr.*, 33(5), 1176-1182.

Buchwald, C., A. E. Santoro, R. H. Stanley, and K. L. Casciotti (2015), Nitrogen cycling in the secondary nitrite maximum of the eastern tropical North Pacific off Costa Rica, *Global Biogeochemical Cycles*, 29(12), 2061-2081.

Casciotti, K. L., C. Buchwald, and M. McIlvin (2013), Implications of nitrate and nitrite isotopic measurements for the mechanisms of nitrogen cycling in the Peru oxygen deficient zone, *Deep Sea Res. I*, 80, 78-93.

- 1044 Casciotti, K. L., J. K. Bohlke, M. R. McIlvin, S. J. Mroczkowski, and J. E. Hannon (2007),
1045 Oxygen isotopes in nitrite: Analysis, calibration, and equilibration, *Anal. Chem.*,
1046 79(6), 2427-2436.
- 1047 Codispoti, L., and J. Christensen (1985), Nitrification, denitrification and nitrous oxide
1048 cycling in the eastern tropical South Pacific Ocean, *Mar. Chem.*, 16(4), 277-300.
- 1049 Cohen, Y., and L. Gordon (1979), Nitrous oxide production in the ocean, *J. Geophys. Res.*,
1050 84, 347-353.
- 1051 Dekaezemacker, J., S. Bonnet, O. Grosso, T. Moutin, M. Bressac, and D. Capone (2013),
1052 Evidence of active dinitrogen fixation in surface waters of the eastern tropical South
1053 Pacific during El Niño and La Niña events and evaluation of its potential nutrient
1054 controls, *Global Biogeochemical Cycles*, 27(3), 768-779.
- 1055 Devol, A. H. (2008), Denitrification including Anammox, in *Nitrogen in the Marine*
1056 *Environment*, edited by D. G. Capone, D. A. Bronk, M. R. Mulholland and E. J.
1057 Carpenter, pp. 263-301, Academic Press.
- 1058 Dugdale, R. C., and J. J. Goering (1967), Uptake of new and regenerated forms of nitrogen in
1059 primary productivity, *Limnol. Oceanogr.*, 12(2), 196-206.
- 1060 Dytczak, M. A., K. L. Londry, and J. A. Oleszkiewicz (2008), Activated sludge operational
1061 regime has significant impact on the type of nitrifying community and its nitrification
1062 rates, *Water research*, 42(8-9), 2320-2328.
- 1063 Edwards, B., D. Murphy, C. Janzen, and N. Larson (2010), Calibration, response, and
1064 hysteresis in deep-sea dissolved oxygen measurements, *Journal of Atmospheric and*
1065 *Oceanic Technology*, 27, 920-931.
- 1066 Farias, L., M. Castro-Gonzalez, M. Cornejo, J. Charpentier, J. Faundez, N. Boontanon, and N.
1067 Yoshida (2009), Denitrification and nitrous oxide cycling within the upper oxycline of
1068 the eastern tropical South Pacific oxygen minimum zone, *Limnol. Oceanogr.*, 54, 132-
1069 144.
- 1070 Farías, L., V. Besoain, and S. García-Loyola (2015), Presence of nitrous oxide hotspots in the
1071 coastal upwelling area off central Chile: an analysis of temporal variability based on
1072 ten years of a biogeochemical time series, *Environmental Research Letters*, 10(4),
1073 044017.
- 1074 Frame, C., and K. Casciotti (2010), Biogeochemical controls and isotopic signatures of
1075 nitrous oxide production by a marine ammonia-oxidizing bacterium, *Biogeosciences*,
1076 7, 2695-2709.
- 1077 Fuchsman, C. A., A. H. Devol, J. K. Saunders, C. McKay, and G. Rocap (2017), Niche
1078 Partitioning of the N cycling microbial community of an offshore Oxygen Deficient
1079 Zone, *Frontiers in microbiology*, 8, 2384.
- 1080 Ganesh, S., D. J. Parris, E. F. DeLong, and F. J. Stewart (2014), Metagenomic analysis of
1081 size-fractionated picoplankton in a marine oxygen minimum zone, *ISME J.*, 8(1), 187-
1082 211.
- 1083 Ganesh, S., L. A. Bristow, M. Larsen, N. Sarode, B. Thamdrup, and F. J. Stewart (2015),
1084 Size-fraction partitioning of community gene transcription and nitrogen metabolism in
1085 a marine oxygen minimum zone, *The ISME journal*, 9(12), 2682.
- 1086 Glibert, P., F. Lipschultz, J. McCarthy, and M. Altabet (1982), Isotope dilution models of
1087 uptake and remineralization of ammonium by marine plankton, *Limnol. Oceanogr.*,
1088 27(4), 639-650.

1089 Goreau, T. J., W. A. Kaplan, S. C. Wofsy, M. B. McElroy, F. W. Valois, and S. W. Watson
1090 (1980), Production of NO₂- and N₂O by nitrifying bacteria at reduced concentrations
1091 of oxygen, *Appl. Environ. Microbiol.*, *40*, 526-532.

1092 Granger, J., and S. D. Wankel (2016), Isotopic overprinting of nitrification on denitrification
1093 as a ubiquitous and unifying feature of environmental nitrogen cycling, *Proceedings of*
1094 *the National Academy of Sciences*, *113*(42), E6391-E6400.

1095 Granger, J., D. M. Sigman, M. G. Prokopenko, M. F. Lehmann, and P. D. Tortell (2006), A
1096 method for nitrite removal in nitrate N and O isotope analyses, *Limnology and*
1097 *OceanographyMethods*, *4*(3432), 205-212.

1098 Haskell, W. Z., W. M. Berelson, D. E. Hammond, and D. G. Capone (2013), Particle sinking
1099 dynamics and POC fluxes in the Eastern Tropical South Pacific based on 234Th
1100 budgets and sediment trap deployments, *Deep Sea Res. I*, *81*, 1-13.

1101 Haskell, W. Z., D. Kadko, D. E. Hammond, A. N. Knapp, M. G. Prokopenko, W. M.
1102 Berelson, and D. G. Capone (2015), Upwelling velocity and eddy diffusivity from 7Be
1103 measurements used to compare vertical nutrient flux to export POC flux in the Eastern
1104 Tropical South Pacific, *Mar. Chem.*, *168*, 140-150.

1105 Ho, D. T., C. S. Law, M. J. Smith, P. Schlosser, M. Harvey, and P. Hill (2006), Measurements
1106 of air - sea gas exchange at high wind speeds in the Southern Ocean: Implications for
1107 global parameterizations, *Geophys. Res. Lett.*, *33*(16).

1108 Holmes, R. M., A. Aminot, R. K rouel, B. A. Hooker, and B. J. Peterson (1999), A simple
1109 and precise method for measuring ammonium in marine and freshwater ecosystems,
1110 *Canadian Journal of Fisheries and Aquatic Sciences*, *56*(10), 1801-1808.

1111 Horak, R. E., W. Qin, A. D. Bertagnolli, A. Nelson, K. R. Heal, H. Han, M. Heller, A. J.
1112 Schauer, W. H. Jeffrey, and E. V. Armbrust (2018), Relative impacts of light,
1113 temperature, and reactive oxygen on thaumarchaeal ammonia oxidation in the North
1114 Pacific Ocean, *Limnol. Oceanogr.*, *63*(2), 741-757.

1115 Jacob, J., B. Nowka, V. Merten, T. Sanders, E. Spieck, and K. D hnke (2017), Oxidation
1116 kinetics and inverse isotope effect of marine nitrite-oxidizing isolates, *Aquat. Microb.*
1117 *Ecol.*, *80*(3), 289-300.

1118 Ji, Q. X., A. R. Babbin, A. Jayakumar, S. Oleynik, and B. B. Ward (2015), Nitrous oxide
1119 production by nitrification and denitrification in the Eastern Tropical South Pacific
1120 oxygen minimum zone, *Geophys. Res. Lett.*, *42*(24), 10755-10764.

1121 Ji, Q. X., E. Buitenhuis, P. Suntharalingam, J. L. Sarmiento, and B. B. Ward (2018), Global
1122 Nitrous Oxide Production Determined by Oxygen Sensitivity of Nitrification and
1123 Denitrification, *Global Biogeochemical Cycles*, *32*(12), 1790-1802.

1124 Johnson, M. T., P. S. Liss, T. G. Bell, T. J. Lesworth, A. R. Baker, A. J. Hind, T. D. Jickells,
1125 K. F. Biswas, E. M. S. Woodward, and S. W. Gibb (2008), Field observations of the
1126 ocean-atmosphere exchange of ammonia: Fundamental importance of temperature as
1127 revealed by a comparison of high and low latitudes, *Global Biogeochemical Cycles*,
1128 *22*(1).

1129 Jung, M.-Y., J.-H. Gwak, L. Rohe, A. Giesemann, J.-G. Kim, R. Well, E. L. Madsen, C. W.
1130 Herbold, M. Wagner, and S.-K. Rhee (2019), Indications for enzymatic denitrification
1131 to N₂O at low pH in an ammonia-oxidizing archaeon, *The ISME journal*, *1*.

1132 Kalvelage, T., G. Lavik, P. Lam, S. Contreras, L. Arteaga, C. R. L scher, A. Oschlies, A.
1133 Paulmier, L. Stramma, and M. M. Kuypers (2013), Nitrogen cycling driven by organic
1134 matter export in the South Pacific oxygen minimum zone, *Nat Geosci*, *6*(3), 228.

1135 Kitzinger, K., H. K. Marchant, L. A. Bristow, C. W. Herbold, C. C. Padilla, A. T. Kidane, S.
 1136 Littmann, H. Daims, P. Pjevac, and F. J. Stewart (2020), Single cell analyses reveal
 1137 contrasting life strategies of the two main nitrifiers in the ocean, *Nature*
 1138 *communications*, *11*(1), 1-12.
 1139 Knapp, A. N., K. L. Casciotti, W. M. Berelson, M. G. Prokopenko, and D. G. Capone (2016),
 1140 Low rates of nitrogen fixation in eastern tropical South Pacific surface waters,
 1141 *Proceedings of the National Academy of Sciences*, *113*(16), 4398-4403.
 1142 Kozłowski, J. A., M. Stieglmeier, C. Schleper, M. G. Klotz, and L. Y. Stein (2016), Pathways
 1143 and key intermediates required for obligate aerobic ammonia-dependent
 1144 chemolithotrophy in bacteria and Thaumarchaeota, *ISME J*, *10*(8), 1836-1845.
 1145 Lam, P., M. M. Jensen, G. Lavik, D. F. McGinnis, B. Muller, C. J. Schubert, R. Amann, B.
 1146 Thamdrup, and M. M. M. Kuypers (2007), Linking crenarchaeal and bacterial
 1147 nitrification to anammox in the Black Sea, *Proc. Natl. Acad. Sci. U. S. A.*, *104*(17),
 1148 7104-7109.
 1149 Lam, P., G. Lavik, M. M. Jensen, J. van de Vossenberg, M. Schmid, D. Woebken, D.
 1150 Guti rrez, R. Amann, M. S. M. Jetten, and M. M. M. Kuypers (2009), Revising the
 1151 nitrogen cycle in the Peruvian oxygen minimum zone, *Proceedings of the National*
 1152 *Academy of Sciences*, *106*(12), 4752.
 1153 Lipschultz, F., S. C. Wofsy, B. B. Ward, L. A. Codispoti, G. E. Friederich, and J. W. Elkins
 1154 (1990), Bacterial transformations of inorganic nitrogen in the oxygen-deficient waters
 1155 of the Eastern Tropical South Pacific Ocean, *Deep Sea Research*, *37*(10), 1513-1541.
 1156 Liu, S., P. Han, L. Hink, J. I. Prosser, M. Wagner, and N. Bruggemann (2017), Abiotic
 1157 conversion of extracellular NH₂OH contributes to N₂O emission during ammonia
 1158 oxidation, *Environ. Sci. Technol.*, *51*(22), 13122-13132.
 1159 Lomas, M. W., and F. Lipschultz (2006), Forming the primary nitrite maximum: Nitrifiers or
 1160 phytoplankton?, *Limnol. Oceanogr.*, *51*(5), 2453-2467.
 1161 L scher, C., A. Kock, M. Koenneke, J. LaRoche, H. Bange, and R. Schmitz-Streit (2012),
 1162 Production of oceanic nitrous oxide by ammonia-oxidizing archaea, *Biogeosciences*,
 1163 *9*, 2419-2429.
 1164 Martin, J. H., G. A. Knauer, D. M. Karl, and W. W. Broenkow (1987), Vertex - Carbon
 1165 Cycling in the Northeast Pacific, *Deep Sea Res. I*, *34*(2), 267-285.
 1166 Martinez-Rey, J., L. Bopp, M. Gehlen, A. Tagliabue, and N. Gruber (2015), Projections of
 1167 oceanic N₂O emissions in the 21st century using the IPSL Earth system model,
 1168 *Biogeosciences (BG)*, *12*(13), 4133-4148.
 1169 McIlvin, M. R., and M. A. Altabet (2005), Chemical conversion of nitrate and nitrite to
 1170 nitrous oxide for nitrogen and oxygen isotopic analysis in freshwater and seawater,
 1171 *Anal. Chem.*, *77*(17), 5589-5595.
 1172 McIlvin, M. R., and K. L. Casciotti (2010), Fully automated system for stable isotopic
 1173 analysis of dissolved nitrous oxide at natural abundance levels, *Limnology and*
 1174 *Oceanography Methods*, *8*, 54-66.
 1175 McIlvin, M. R., and K. L. Casciotti (2011), Technical updates to the bacterial method for
 1176 nitrate isotopic analyses, *Anal. Chem.*, *83*(5), 1850-1856.
 1177 Mincer, T. J., M. J. Church, L. T. Taylor, C. Preston, D. M. Karl, and E. F. DeLong (2007),
 1178 Quantitative distribution of presumptive archaeal and bacterial nitrifiers in Monterey
 1179 Bay and the North Pacific Subtropical Gyre, *Environ. Microbiol.*, *9*(5), 1162-1175.

1180 Mosier, A. C., and C. A. Francis (2011), Determining the distribution of marine and coastal
1181 ammonia-oxidizing archaea and bacteria using a quantitative approach, *Methods*
1182 *Enzymol.*, 486, 205-221.

1183 Nevison, C., J. H. Butler, and J. Elkins (2003), Global distribution of N₂O and the DN₂O-
1184 AOU yield in the subsurface ocean, *Global Biogeochem. Cycles*, 17(4), 1119.

1185 Nevison, C. D., R. F. Weiss, and D. J. Erickson III (1995), Global oceanic emissions of
1186 nitrous oxide, *Journal of Geophysical Research: Oceans*, 100(C8), 15809-15820.

1187 Newell, S. E., A. R. Babbin, A. Jayakumar, and B. B. Ward (2011), Ammonia oxidation rates
1188 and nitrification in the Arabian Sea, *Global Biogeochemical Cycles*, 25, Gb4016.

1189 Owens, S., S. Pike, and K. Buesseler (2015), Thorium-234 as a tracer of particle dynamics
1190 and upper ocean export in the Atlantic Ocean, *Deep Sea Res. II*, 116, 42-59.

1191 Paulot, F., D. J. Jacob, M. T. Johnson, T. G. Bell, A. R. Baker, W. C. Keene, I. D. Lima, S. C.
1192 Doney, and C. A. Stock (2015), Global oceanic emission of ammonia: Constraints
1193 from seawater and atmospheric observations, *Global Biogeochemical Cycles*, 29(8),
1194 1165-1178.

1195 Peng, X., C. A. Fuchsman, A. Jayakumar, S. Oleynik, W. Martens - Habbena, A. H. Devol,
1196 and B. B. Ward (2015), Ammonia and nitrite oxidation in the Eastern Tropical North
1197 Pacific, *Global Biogeochemical Cycles*, 29(12), 2034-2049.

1198 Peng, X. F., C. A. Fuchsman, A. Jayakumar, M. J. Warner, A. H. Devol, and B. B. Ward
1199 (2016), Revisiting nitrification in the Eastern Tropical South Pacific: A focus on
1200 controls, *J. Geophys. Res.*, 121(3), 1667-1684.

1201 Ploug, H., and J. Bergkvist (2015), Oxygen diffusion limitation and ammonium production
1202 within sinking diatom aggregates under hypoxic and anoxic conditions, *Mar. Chem.*,
1203 176, 142-149.

1204 Prairie, J. C., K. Ziervogel, R. Camassa, R. M. McLaughlin, B. L. White, Z. I. Johnson, and
1205 C. Arnosti (2017), Ephemeral aggregate layers in the water column leave lasting
1206 footprints in the carbon cycle, *Limnology and Oceanography Letters*, 2(6), 202-209.

1207 Qin, W., K. A. Meinhardt, J. W. Moffett, A. H. Devol, E. V. Armbrust, A. E. Ingalls, and D.
1208 A. Stahl (2017), Influence of oxygen availability on the activities of ammonia-
1209 oxidizing archaea, *Environmental Microbiology Reports*, 9(3), 250-256.

1210 Raimbault, P., N. Garcia, and F. Cerutti (2008), Distribution of inorganic and organic
1211 nutrients in the South Pacific Ocean-evidence for long-term accumulation of organic
1212 matter in nitrogen-depleted waters, *Biogeosciences*, 5(2), 281-298.

1213 Santoro, A. E., K. L. Casciotti, and C. A. Francis (2010), Activity, abundance and diversity of
1214 nitrifying archaea and bacteria in the central California Current, *Environ. Microbiol.*,
1215 12, 1989-2006.

1216 Santoro, A. E., C. Buchwald, M. R. McIlvin, and K. L. Casciotti (2011), Isotopic composition
1217 of N₂O produced by marine ammonia-oxidizing archaea, *Science*, 333, 1282.

1218 Santoro, A. E., M. A. Saito, T. J. Goepfert, C. H. Lamborg, C. L. Dupont, and G. R. DiTullio
1219 (2017), Thaumarchaeal ecotype distributions across the equatorial Pacific Ocean and
1220 their potential roles in nitrification and sinking flux attenuation, *Limnol. Oceanogr.*,
1221 62(5), 1984-2003.

1222 Santoro, A. E., C. M. Sakamoto, J. M. Smith, J. N. Plant, A. L. Gehman, A. Z. Worden, K. S.
1223 Johnson, C. A. Francis, and K. L. Casciotti (2013), Measurements of nitrite production
1224 in and around the primary nitrite maximum in the central California Current,
1225 *Biogeosciences*, 10(11), 7395-7410.

1226 Santoro, A. E., C. L. Dupont, R. A. Richter, M. T. Craig, P. Carini, M. R. McIlvin, Y. Yang,
1227 W. D. Orsi, D. M. Moran, and M. A. Saito (2015), Genomic and proteomic
1228 characterization of “Candidatus Nitrosopelagicus brevis”: An ammonia-oxidizing
1229 archaeon from the open ocean, *Proc. Natl. Acad. Sci. U. S. A.*, 112(4), 1173-1178.

1230 Sigman, D. M., K. L. Casciotti, M. Andreani, C. Barford, M. Galanter, and J. K. Bohlke
1231 (2001), A bacterial method for the nitrogen isotopic analysis of nitrate in seawater and
1232 freshwater, *Anal. Chem.*, 73(17), 4145-4153.

1233 Sigman, D. M., J. Granger, P. J. DiFiore, M. F. Lehmann, R. Ho, G. Cane, and A. van Geen
1234 (2005), Coupled nitrogen and oxygen isotope measurements of nitrate along the
1235 eastern North Pacific margin, *Global Biogeochem. Cycles*, 19(4), GB4022.

1236 Smith, J. M., F. P. Chavez, and C. A. Francis (2014a), Ammonium uptake by phytoplankton
1237 regulates nitrification in the sunlit ocean, *Plos One*, 9(9), e108173.

1238 Smith, J. M., K. L. Casciotti, F. P. Chavez, and C. A. Francis (2014b), Differential
1239 contributions of archaeal ammonia oxidizer ecotypes to nitrification in coastal surface
1240 waters, *ISME J*, 8(8), 1704-1714.

1241 Smith, J. M., J. Damascheck, F. P. Chavez, and C. A. Francis (2015), Factors influencing
1242 nitrification rates and the abundance and transcriptional activity of ammonia-oxidizing
1243 microorganisms in the dark northeast Pacific Ocean, *Limnol. Oceanogr.*

1244 Stieglmeier, M., M. Mooshammer, B. Kitzler, W. Wanek, S. Zechmeister-Boltenstern, A.
1245 Richter, and C. Schleper (2014), Aerobic nitrous oxide production through N-
1246 nitrosating hybrid formation in ammonia-oxidizing archaea, *ISME J*, 8(5), 1135-1146.

1247 Strickland, J., and T. Parsons (1968), A practical handbook of seawater analysis, *Fisheries*
1248 *Research Board of Canada Bulletin*, 167, 71-75.

1249 Sun, X., L. F. Kop, M. C. Lau, J. Frank, A. Jayakumar, S. Lücker, and B. B. Ward (2019),
1250 Uncultured Nitrospina-like species are major nitrite oxidizing bacteria in oxygen
1251 minimum zones, *The ISME journal*, 13(10), 2391-2402.

1252 Suntharalingam, P., J. Sarmiento, and J. Toggweiler (2000), Global significance of nitrous-
1253 oxide production and transport from oceanic low-oxygen zones: A modeling study,
1254 *Global Biogeochemical Cycles*, 14(4), 1353-1370.

1255 Taylor, B. W., C. F. Keep, R. O. Hall, B. J. Koch, L. M. Tronstad, A. S. Flecker, and A. J.
1256 Ulseth (2007), Improving the fluorometric ammonium method: matrix effects,
1257 background fluorescence, and standard additions, *J N Am Benthol Soc*, 26(2), 167-177.

1258 Trimmer, M., P. M. Chronopoulou, S. T. Maanoja, R. C. Upstill-Goddard, V. Kitidis, and K.
1259 J. Purdy (2016), Nitrous oxide as a function of oxygen and archaeal gene abundance in
1260 the North Pacific, *Nature Communications*, 7.

1261 Wanninkhof, R. (1992), Relationship between wind speed and gas exchange, *J. Geophys. Res.*,
1262 97(25), 7373-7382.

1263 Ward, B., A. Devol, J. Rich, B. Chang, S. Bulow, H. Naik, A. Pratihary, and A. Jayakumar
1264 (2009), Denitrification as the dominant nitrogen loss process in the Arabian Sea,
1265 *Nature*, 461(7260), 78-81.

1266 Ward, B. B. (2008), Nitrification in Marine Systems, in *Nitrogen in the Marine Environment*,
1267 edited by D. G. Capone, D. A. Bronk, M. R. Mulholland and E. J. Carpenter, pp. 199-
1268 262, Elsevier.

1269 Ward, B. B., and O. C. Zafiriou (1988), Nitrification and nitric oxide in the oxygen minimum
1270 of the eastern tropical North Pacific, *Deep Sea Res. I*, 35(7), 1127-1142.

1271 Ward, B. B., H. E. Glover, and F. Lipschultz (1989), Chemoautotrophic activity and
1272 nitrification in the oxygen minimum zone off Peru, *Deep Sea Res. I*, 36(7), 1031-1051.
1273 Winkler, M.-K., Q. H. Le, and E. I. Volcke (2015), Influence of partial denitrification and
1274 mixotrophic growth of NOB on microbial distribution in aerobic granular sludge,
1275 *Environ. Sci. Technol.*, 49(18), 11003-11010.
1276 Wuchter, C., et al. (2006), Archaeal nitrification in the ocean, *Proc. Natl. Acad. Sci. U. S. A.*,
1277 103(33), 12317-12322.
1278 Yang, S., et al. (in press), Global reconstruction reduces the uncertainty of oceanic nitrous
1279 oxide emissions and reveals a vigorous seasonal cycle, *Proceedings of the National*
1280 *Academy of Sciences*.
1281 Yeung, L. Y., W. M. Berelson, D. E. Hammond, M. G. Prokopenko, C. Wolfe, and N. Rollins
1282 (2015), Upper-ocean gas dynamics from radon profiles in the Eastern Tropical South
1283 Pacific, *Deep Sea Res. I*, 99, 35-45.
1284 Yoshida, N., H. Morimoto, M. Hirano, I. Koike, S. Matsuo, E. Wada, T. Saino, and A. Hattori
1285 (1989), Nitrification rates and ¹⁵N abundances of N₂O and NO₃⁻ in the western North
1286 Pacific, *Nature*, 342, 895-897.
1287 Zafiriou, O. C., and M. B. True (1979), Nitrate photolysis in seawater by sunlight, *Mar.*
1288 *Chem.*, 8(1), 33-42.
1289 Zakem, E. J., A. Al-Haj, M. J. Church, G. L. Dijken, S. Dutkiewicz, S. Q. Foster, R. W.
1290 Fulweiler, M. M. Mills, and M. J. Follows (2018), Ecological control of nitrite in the
1291 upper ocean, *Nature communications*, 9(1), 1206.
1292 Zamora, L., A. Oschlies, H. Bange, K. Huebert, J. Craig, A. Kock, and C. Löscher (2012),
1293 Nitrous oxide dynamics in low oxygen regions of the Pacific: insights from the
1294 MEMENTO database, *Biogeosciences*, 9(12), 5007-5022.
1295